ICAM

Institute for Computational and Applied Mechanics

ANALYSIS OF PULTRUSION PROCESSING FOR LONG FIBER REINFORCED THERMOPLASTIC COMPOSITE SYSTEM

By

W. Tso, T. H. Hou, and S. N. Tiwari

NASA Grant NAG-1-363
NASA Langley Research Center
Hampton, Virginia 23681-0001

ODU/ICAM Report 93-103
November 1993

Old Dominion University
Norfolk, Virginia 23529-0247

ABSTRACT

ANALYSIS OF PULTRUSION PROCESSING FOR LONG FIBER REINFORCED THERMOPLASTIC COMPOSITE SYSTEM

Pultrusion is one of the composite processing technology, commonly recognized as a simple and cost-effective means for the manufacturing of fiber-reinforced, resin matrix composite parts with different regular geometries. Previously, because the majority of the pultruded composite parts were made of thermosetting resin matrix, emphasis of the analysis on the process has been on the conservation of energy from various sources, such as heat conduction and the curing kinetics of the resin system. Analysis on the flow aspect of the process was almost absent in the literature for thermosetting process. With the increasing uses of thermoplastic materials, it is desirable to obtain the detailed velocity and pressure profiles inside the pultrusion die. Using a modified Darcy's law for flow through porous media, closed form analytical solutions for the velocity and pressure distributions inside the pultrusion die are obtained for the first time. This enables us to estimate the magnitude of viscous dissipation and its effects on the pultruded parts. Pulling forces refined in the pultrusion processing are also analyzed. The analytical model derived in this study can be used to advance our knowledge and control of the pultrusion process for fiber reinforced thermoplastic composite parts.

TABLE OF CONTENTS

ACKNOWLEDGEMENTS

This research was conducted in cooperation with the Polymeric Materials Branch (Materials Division) of the NASA Langley Research Center during the period of January 1991 to December 1992. A part of this work constituted as a Master's Thesis for Mr. Wen Tso in the Mechanical Engineering Department at Old Dominion University. Certain modifications were made in thesis materials during the spring and summer of 1993. The report, in the present form, became available in September 1993.

The authors are indebted to Drs. Gene W. Hou of Old Dominion University, and Terry L. St. Clair of NASA Langley, for their cooperation and technical assistance. Partial funding for this research was provided by the NASA Langley Research Center through the ICAM Program in Aeronautics, Grant NAG-1-363. The grant was monitored by Mr. Robert L. Yang, Assistant University Affairs Officer, Mail Stop 400, NASA Langley Research Center, Hampton, Virginia 23681-0001.

LIST OF TABLES

LIST OF FIGURES

LIST OF SYMBOLS

$A(z)$	Cross section of the pultrusion die
B_r	Brinkman Number
$\mathbf{D}$	Matrix with derivatives of shape function
D_f	Fiber filament diameter
$f(r)$	$(v_z(z,r)-v_f)/z$, a function of r only
$\mathbf{F}$	Viscous force matrix
F_c	Collimation forces contribution to the total pulling force
F_c^b	Resin backflow contributions to the collimation forces F_c
F_c^c	Bulk compaction contributions to the collimation forces F_c
F_c^T	Thermally induced contributions to the collimation forces F_c
F_f	Friction forces contribution to the total pulling force
F_f^I	Hydrostatic pressure contributions to the friction forces F_f
F_f^{II}	Normal stress contribution to the friction forces F_f
F_f^{III}	Fiber compaction contribution to the friction forces F_f
F_{tot}	Total pulling force for the composite laminate pultrusion
F_v	Viscous drag contribution to the total pulling force
$\mathbf{H}$	Constant vector with velocity gradient nodal values
$h(\infty)$	Minimum Attainable thickness of the fiber mat
I_0	Modified Bessel Function of zero order of the first kind
I_1	Modified Bessel Function of one order of the first kind

$\mathbf{J}$	Jacobian matrix
$\mathbf{J}^{-1}$	Inverse of Jacobian matrix
$\mathbf{J}_1$, $\mathbf{J}_2$	First and second rows of Jacobian matrix
JJ	2×2 matrix
$\mathbf{K}$	Stiffness matrix
$\mathbf{K}_a$	Convective matrix
$\mathbf{K}_b$	Conductivity matrix
K_c	Coefficient of conductivity
K_{FENE}	Finitely Extendable Nonlinear Elastic spring constant
k_z	Permeability in the fiber direction
k_r	Permeability in the transverse direction of the fiber bundle
L	Length of the main die
$\mathbf{L}$	Vector with component of first row of Jacobian matrix
n	Exponential constant of the FENE spring
$\mathbf{N}$	Matrix with shape functions
p(z)	Processing generated pressure profile along the main pultrusion section of the die entrance
$P_b(z)$	Pressure profile due to the backflow along the tapered section of the die section
P_r	Prandtl Number
$P_T(z)$	Thermally induced pressure
Q_b	Backflow volume of flow through the tapered die section
R	Inlet radius of the main pultrusion die section
R_e	Reynolds Number
s, t	Variables representing gaussian points

S_z	Konezy constant
$\mathbf{T}$	Nodal temperature vector
T_{amb}	Ambient temperature
T_{pul}	Isothermal pultrusion die temperature
v_f	Pulling speed of the pultrusion processing
$\mathbf{V}$	Constant vector with velocity nodal value
V_o	Incoming volume fraction of the fiber bundles at the $z=-\alpha L$
$V_f(z)$	Volume fraction of the fiber bundles along the pultrusion die
$V_r(r)$	Resin velocity in the r-direction inside the die
$V_z(z,r)$	Resin velocity in the z-direction inside the die
W_i	Weighting coefficients
z, r, θ	Cylindrical coordinate system fixed on the inlet of the Main pultrusion die section
αL	Length of the entry die
α_v	Coefficient of the thermal expansion of the resin
ϵ	Related to contraction ratio of the tapered section near the die entrance
ϵR	Inlet radius of the tapered section near entrance
Θ	Multiplication of Jacobian matrix and its determinant
κ_c	Compressibility of the resin
λ	Contraction ratio of the main pultrusion section of the die which is only mildly tapered. λ=0.98 is given for this investigation

λR	Exit radius of the main pultrusion die section
μ	Resin viscosity
ϕ	Taper angle of the die near entrance ($\phi=\tan^{-1}[(\epsilon-1)/\alpha]>0$)
Ω^e	Integration domain

Chapter 1

INTRODUCTION

1.1 Preview and Literature Survey

The demands for stronger, tougher, higher temperature resistant thermoplastic composites has increased dramatically in recent years. Thus, the pultrusion technology faces many new challenges. Since 1957, over 130 papers dealing with subjects related to the pultrusion process, such as product and tooling designs, raw materials, machinery, product markets, etc. have appeared. However, few investigations dealt with in-depth analysis of the flow field inside the pultrusion die. Because of the lack of basic understanding of the stress and strain fields generated by the pultruded laminate part inside the heated die, most pultrusion processing was still operated on a trial and error basis. Such a practice leads to frequent fiber breakages and process down-times.

The previous works focused on the physical and chemical properties of thermosetting resin systems. For this type of resin system, prediction of the temperature inside the pultrusion die requires accurate reaction kinetics and material properties. The equations of reaction kinetics for a variety of chemical systems are often nonlinear. When coupled to the heat transfer to and from the die wall, the resulted equation for conservation of energy is difficult to compute.

Price [1][1] was the first to use a heat-transfer model for pultrusion analysis. Two limiting cases were examined: an isothermal case with a uniform die wall temperature and adiabatic case where heat conduction was negligible. The model used first order

[1] The numbers in brackets indicate reference

kinetics for epoxy resins. No experimental data was provided for the evaluation of modeling results, however.

Tulig [2] used finite elements to model pultrusion cure of epoxy resins in round and irregular die shapes. Boundary conditions was specified to simulate both the heat input from the die heater and heat losses due to convection with air. Tulig's work is the only published model to date which has been successfully verified with experimental data for epoxy resin.

Han, et al. [3] used an autocatalytic model for unsaturated polyesters and epoxies, and allow density, thermal conductivity and heat capacity to change with degree of cure. No experimental data was presented, however.

Ma, et al. [4] published a model similar to Han, but, for the first time, axial conduction along the pultrusion die was included in the calculations. No evidence was given, however, to show that axial conduction was significant.

Batch and Macosko [5] used a mechanistic kinetic model for polyesters which included provisions for diffusion-limited chain propagations. Also included in their analysis were models for pressure and pulling force predictions.

The analysis of pultrusion processing currently undertaken and presented below differs from the works mentioned above in two major ways:

(1) This research deals with thermoplastic based composite systems. There is no reaction heat evolved from the processing. In addition to the conduction heat from the die wall, the viscous heating generated in the high shearing zone between the pultrudate and the die is also included in the analysis.

(2) Unlike the conventional assumption, that the pultrusion is equivalent to a plug resin flow reactor, used in literature, detail analyses of the flow and pressure fields inside the pultrusion die are conducted. This analysis also enable one to estimate the extent of viscous heating mentioned in (1) which was unable to be performed by all previous workers.

1.2 Outline

The flow analysis for both the entrance section and the main pultrusion die section is presented in Chap. 2. The detailed pressure distribution is recognized as one of the most significant factors that determine the effect of process. It is also necessary to know that the relationship among the back flow pressure p_b incoming volume fraction V_0 and permeability k.

Chapter 3 covers the motion of the resin and fiber composite. The complete force distributions are given in detail by different mathematical formulas. As a matter of fact, the viscous drag F_v, frictions F_f and collimation force F_c, are affected by the processing parameters, geometry parameters and material parameters.

The viscous heating is what we most expect to know in the thermoplastic pultrusion thermal analysis, distinguishing from the reaction-dominated thermosetting processing. Consequently, the conservation of the equation is derived in Chap. 4.

The finite element analysis is used to analyze the thermal aspect of the pultrusion processing, which is presented in the Chap. 5. The conclusion and the appendix are complemented to discussion in the previous chapters.

Chapter 2

FLOW ANALYSIS OF PULTRUSION PROCESS

2.1 Statement of the Problem

The pultrusion process line consists of several processing steps. They are fiber impregnation, preheating zone, pultruding die and part cutoffs. Among them, the pultruding die is the focal point of this study.

The pultrusion process of continuous fiber reinforced polymeric resin matrix laminate through a cylindrical die is illustrated in Fig. 2.1. The die consists of two sections: a short tapered section with length αL near the entrance and a main pultrusion die section with length L. A Cylindrical Coordinate Systemis is selected with origin fixed in the inlet of the main pultrusion die section. The composite laminate is pulled by a force F entering the die at $z = -\alpha L$ with a constant speed v_f. The contraction ratio of the tapered entrance section is $1/\epsilon$. The main pultrusion die section is mildly tapered with inlet radius R at $z = 0$ and exit radius λR at $z = L$. The value for $\lambda = 0.98$ is used throughout this investigation. It is desired to obtain the velocity and pressure profiles inside the entire pultrusion die, $-\alpha L \leq z \leq L$, such that the pulling forces required for the processing of thermoplastic composite laminate can be better estimated analytically.

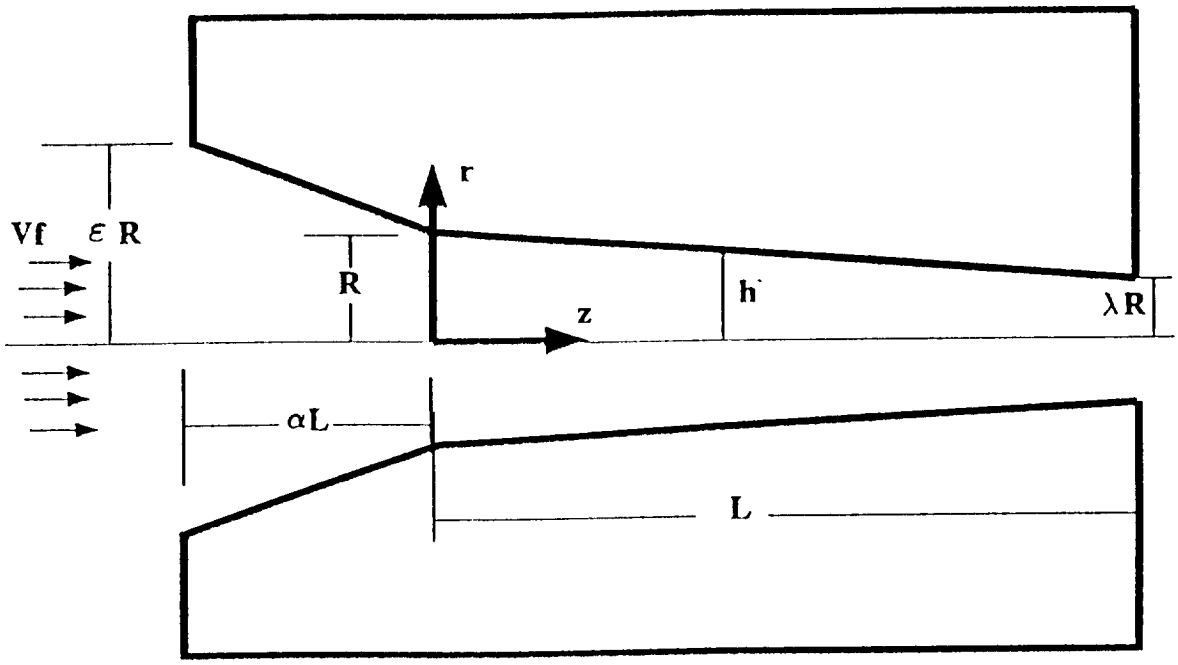

Fig. 2.1 Geometry of Pultrusion System(die).

2.2 Flow Analysis in the Entrance Section

2.2.1 Assumption

The flow inside the entrance tapered section of the die can be analyzed as a flow through porous fiber bundle media with the following assumptions:

1. Portions of the incoming fluid volume which are pultruded through the die, i.e., excluding the backflow volume, travel with the same line speed of the fiber bundles throughout the entrance section. This is a plug flow assumption.

2. Backflow volume is estimated solely from the volume contraction of the flow by the tapered die geometry.

3. One dimensional (in –z direction) Darcy's law is applied, i.e., $v_z = v_z(z)$ only for the backflows. Because the entrance section is short, secondary flows, $v_r(z,r)$, due to the tapered geometry, is negligible. This allows to obtain a simple analytical estimate of the backflow effect.

4. The process is isothermal and in a steady state. There is a uniform viscosity without chemical reactions.

5. Following dimensionless terms are defined as

$$\underline{D}_f = D_f/R, \underline{V}_{bz} = V_{bz}/V_f, \underline{k}_z = k_z/R^2, \underline{P}_b = P_b R^2/(\mu L v_f),$$

$$\underline{z} = z/L, \underline{P}_T = P_T k_c, \tilde{\underline{P}}_T = \underline{P}_T R^2/(k_c \mu L v_f), \underline{P}_{en} = \underline{P}_b + \tilde{\underline{P}}_T$$

2.2.2 Back Flow Pressure Distribution $P_b(z)$

The cross section area of the tapered die at z can be obtained from die geometry as

$$r(z) = R - z\left[\frac{(\epsilon - 1)R}{\alpha L}\right] \tag{2.1}$$

and

$$A(z) = \pi\left[R - z\frac{(\epsilon - 1)R}{\alpha L}\right]^2 \tag{2.2}$$

where $-\alpha L \le z \le 0$, and $\epsilon > 1$. One dimensional Darcy's law in the $-z$ direction for the backflow volume is given by

$$- < v_{bz}(z) >= \frac{k_z(z)}{\mu}\frac{dP_b(z)}{dz} \tag{2.3}$$

where the averaged velocity is $- < v_{bz} >= -Q_b(z)/A(z)$. The backflow volume $Q_b(z)$ is estimated at any location z ($-\alpha L \le z \le 0$) based upon assumptions 1 and 2 as

$$\begin{aligned} Q_b(z) &= Q(z) - Q(0) \\ &= v_f[1 - V_f(z)]A(z) - v_f[1 - V_f(0)]A(0) \end{aligned} \tag{2.4}$$

where $V_f(z)$ is the fiber volume fraction and v_f is the pultrusion line speed. It is noted that the backflow volume vanishes at $z = 0$, which is the inlet of the main pultrusion die section. Thus, we have

$$\begin{aligned} < v_{bz}(z) >= & -\frac{Q_b(z)}{A(z)} \\ &= v_f\{[1 - V_f(0)]\frac{A(0)}{A(z)} - [1 - V_f(z)]\} \end{aligned} \tag{2.5}$$

Equation (2.5) was also independently derived by Batch [6]. Because of the tapered geometry, the axial permeability, $k_z(z)$ [16], due to the change of the fiber volume fraction, $V_f(z)$ is given as

$$k_z(z) = \frac{D_f^2}{16Sz}\frac{(1 - V_f(z))^3}{V_f(z)^2} \tag{2.6}$$

with

$$V_f(z) = V_0\left[\frac{A(-\alpha)}{A(z)}\right] \tag{2.7}$$

where $V_0 = V_f(-\alpha)$ is the incoming volume fraction of the fiber bundles. The quantity D_f is the fiber filament diameter and $S_z = 0.7$ is a characteristic parameter of the graphite fiber bundles investigated by Gutowaski [13]. Values of S_z have also been reported to

be 0.68 by Lam and Kardos [14], 0.48 by Williams et al. [15]. Generally, higher values of S_z are observed for close packed arrays of fiber.

Using the dimensionless terms defined before, and neglecting the underscore bars, the relation for the backflow pressure is expressed as

$$P_b(z) = -\int_{-\alpha}^{z} \frac{< v_{bz}(z) >}{k_z(z)} dz \qquad (-\alpha \le z \le 0) \tag{2.8}$$

where

$$< v_{bz}(z) >= \left[\frac{\pi}{A(z)} - 1\right] \tag{2.9}$$

$$k_z(z) = \frac{D_f^2}{16Sz} \frac{(1 - V_f(z))^3}{V_f(z)^2} \tag{2.10}$$

$$V_f(z) = V_0 \left[\frac{A(-\alpha)}{A(z)}\right] = V_0 \left[\frac{\pi \epsilon^2}{A(z)}\right] \tag{2.11}$$

$$A(z) = \pi \left[R - z\frac{(\epsilon - 1)R}{\alpha L}\right]^2 \tag{2.12}$$

with the boundary condition

$$z = -\alpha \, , P_b(-\alpha) = 0 \tag{2.13}$$

It is noted that the dimensionless pressure distribution, $P_b(z)$, is determined by the permeability, $k_z(z)$, only for a given tapered die geometry at the entrance. In order to solve Eq. (2.8), values of V_0, ϵ, α, D_f and S_z have to be first specified.

With R = .125 inch, D_f = .0005 inch and S_z = 1.0, the behaviors of $P_b(z)$ and $k_z(z)$ in the entrance section of the pultrusion die as a function of process variables are tabulated in Table 2.1. It is seen that the permeability, $k_z(0)$, at z = 0 is a function of

the contraction ratio, Eq. (2.11). For a given die geometry defined by a set of α and ϵ, values of $k_z(0)$ decrease with increasing V_0. The backflow pressure, $P_b(0)$, at $z = 0$ is directly proportional to the tapered die length, α, and increases with increasing ϵ and V_0.

An example of change in fiber volume fraction, $V_f(z)$, along entrance section of the pultrusion die is shown in Fig. 2.2. Values of V_f is noted to increase rapidly in this typical die geometry.

Table 2.1 Changes of $P_b(0)$ and $k_z(0)$ in the Entrance Section of the Pultrusion Die as a Function of Process Variables Indicated*

ϵ=1.5 α=0.1			ϵ=1.5 α=0.2			ϵ=1.5 α=0.3		
V_0	$k_z(0)$	$P_b(0)$	V_0	$k_z(0)$	$P_b(0)$	V_0	$k_z(0)$	$P_b(0)$
.05	.00005	193	.05	.00005	387	.05	.00005	580
.1	9×10^{-6}	993	.1	9×10^{-6}	1986	.1	9×10^{-6}	2979
.2	8.2×10^{-7}	7202	.2	8.2×10^{-7}	14405	.2	8.2×10^{-7}	21607
ϵ=2.5 α=0.1			ϵ=2.5 α=0.2			ϵ=2.5 α=0.3		
V_0	$k_z(0)$	$P_b(0)$	V_0	$k_z(0)$	$P_b(0)$	V_0	$k_z(0)$	$P_b(0)$
.02	.000042	143	.02	.000042	288	.02	.000042	432
.05	.000003	1259	.05	.000003	2520	.05	.000003	3779
.1	1.4×10^{-7}	11173	.1	1.4×10^{-7}	22347	.1	1.4×10^{-7}	33521

*R=0.125 in., D_f=0.0005 in. and S_z=1.0.

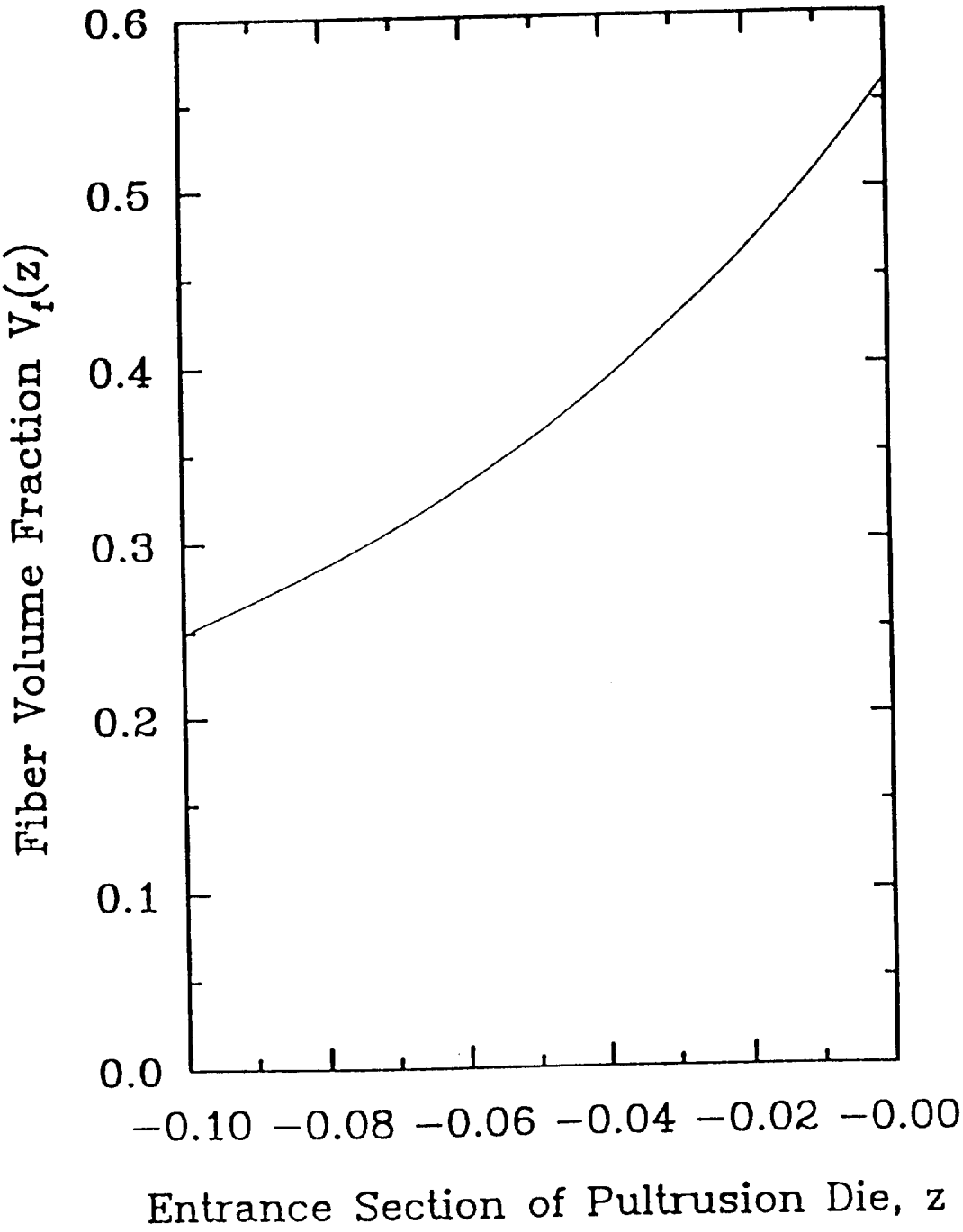

Fig. 2.2 Fiber Volume Fraction; α=0.1, ϵ=1.5, V_o=0.25, R=6.35×10^{-3}m and L=0.3048m.

2.2.3 Thermally Induced Pressurization Distribution $P_T(z)$

For a thermoplastic laminate pultruded through the die, the resin matrix temperature rises continuously, from the ambient temperature T_{amb} to the pultrusion temperature T_{pul}, due to the heat conduction from the die wall. Thermal expansion of the resin system beyond the confinement of the pultrusion die will give rise to a pressurization effect. The amount of the pressure rise due to thermal expansion is related to resin compressibility. By assuming that resin temperature is T = T(r, z), with constant coefficient of thermal expansion α_v and compressibility κ_c, Batch [6] derived the following expression for the thermally induced pressurization effect:

$$P_T(z) = \frac{\alpha_v}{\kappa_c}\left[\overline{T}(z) - T_{amb}\right] \tag{2.14}$$

where the averaged resin temperature is given by

$$\overline{T}(z) = \frac{2}{h^2}\int_0^h T(z,r)rdr \tag{2.15}$$

If we further assume that the resin temperature is uniform over any cross section of the die along z, where $-\alpha L \le z \le L$, and reaches die temperature linearly from $T_0(-\alpha L) = T_{amb}$ to $T(0) = T_{pul}$ at the end of tapered die entrance section (z=0), the dimensionless thermally induced pressure $\underline{P}_T(z)$, as defined above, can be estimated by

$$\underline{P}_T(z) = \alpha_v\left(T_{pul} - T_{amb}\right)\left(1 + \frac{z}{\alpha}\right) \qquad (-\alpha \le z \le 0) \tag{2.16}$$

In order to compare the magnitude of dimensionless pressure contributions on an equal basis, a new dimensionless term $\tilde{\underline{P}}_T$ is required as

$$\tilde{\underline{P}}_T = \underline{P}_T R^2/(\kappa_c \mu L v_f)$$

Consequently, Eq. (2.16) becomes:

$$\tilde{P}_T(z) = \frac{\alpha_v}{\kappa_c}\frac{R^2}{\mu L v_f}(T_{pul} - T_{amb})\left(1 + \frac{z}{\alpha}\right) \qquad (-\alpha \le z \le 0) \tag{2.17}$$

A new dimensionless pressure term is also defined as $\underline{P}_{en}(z) = \underline{P}_b(z) + \underline{\tilde{P}}_T(z)$ which sums up the pressure generated in the entrance tapered die section in the pultrusion process. Using the set of typical values for the pultrusion parameters in Table 2.2, magnitudes of $\underline{P}_b(z)$ and $\underline{\tilde{P}}_T(z)$ are plotted in Fig. 2.3. It is seen that the thermally induced pressurization is a dominant factor for the pressure build-up in the tapered section near the entrance of the pultrusion die. The basestone of making a successful mathematical model is the selection of the parameters which are refined from the experimental data. The type of materials can be categorized as materials parameters, geometry parameters, and processing parameters with given dimensionless or dimensional values.

Table 2.2 Typical Values of Material, Die Geometry and Processing Variables in the Pultrusion Processing

Material parameters		Geometry parameters	
n	1.5	α	0.1
h(∞)	0.87	λ	0.98
V_f(∞)	0.74	ϵ	1.5
μ_f	0.8	R	6.35×10^{-3}m
K_{FENEC}	2.72×10^{7}	L	0.3048m
V_o	0.25	Processing parameters	
D_f	0.002	T_{pul}-T_{amb}	200°C
S_z	1.0	v_f	5.08×10^{-3}m/sec
μ	0.14 PaSec		
α_v	5×10^{-5} °C^{-1}		
κ_c	$5\times10^{-10}m^2N^{-1}$		

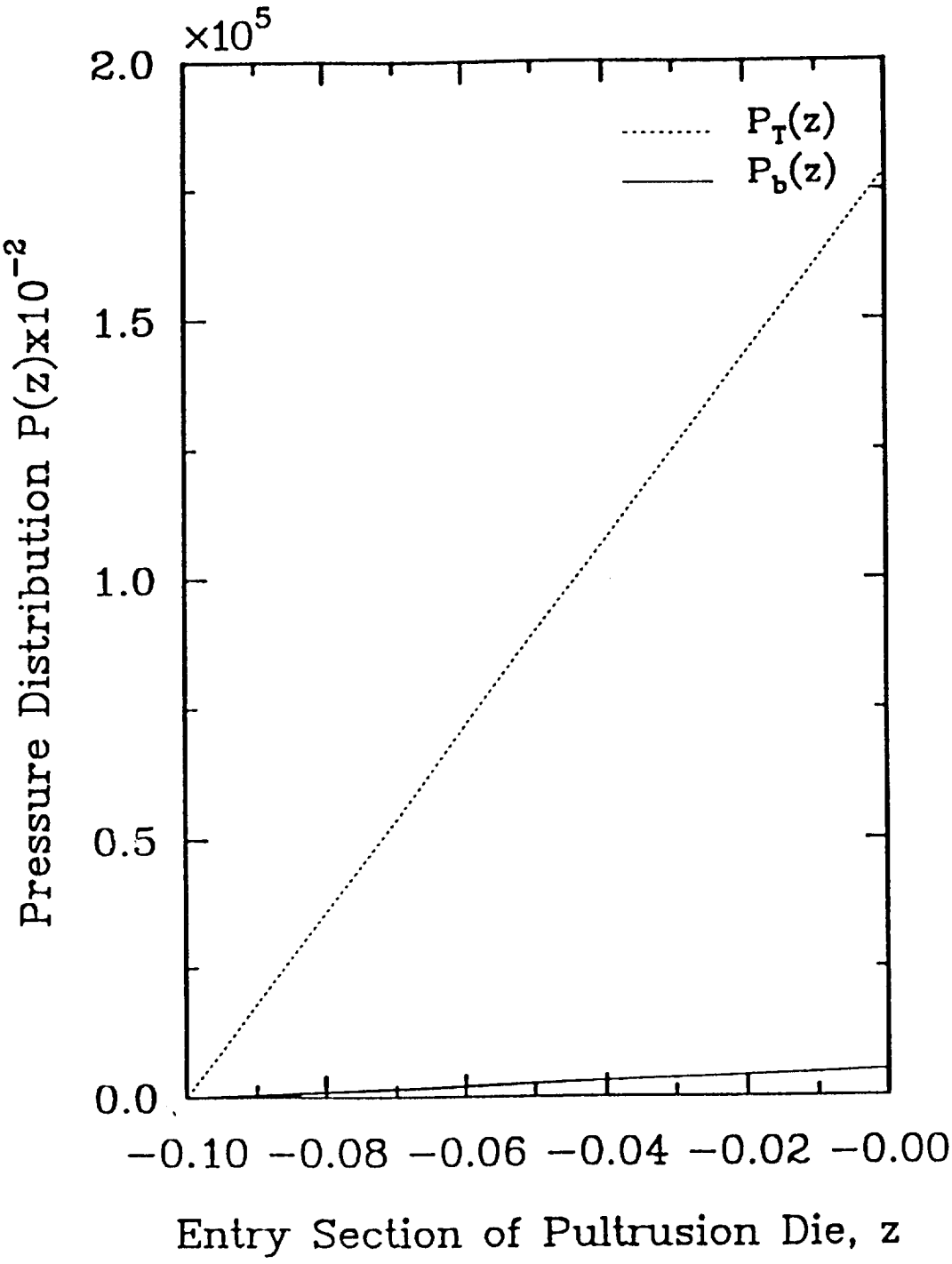

Fig. 2.3 Comparison between Pressure Distribution; α=0.1, ϵ=1.5, V_o=0.25, ΔT=200°C, D_f=0.002, S_z=1, $\alpha_v=5\times10^{-5}\ ^oC^{-1}$, $\kappa_c=5\times10^{-10}m^2N^{-1}$, $\mu=0.14P_aS_{ec}$, R=6.35×10^{-3}m, L=0.3048m and $v_f=6.35\times10^{-3}$m/sec.

2.3 Flow Analysis in the Main Pulrusion Die Section

2.3.1 Assumption

The flow inside the main pultrusion die section can be analyzed as a flow through porous fiber bundle media with the following assumptions:

1. The inlet of the main pultrusion section is the end of the tapered section near the die entrance. Following the assumption 1 specified for the analysis of the tapered section, we have a flat inlet velocity profile with a magnitude of $v_z(0,r) = v_f$, the same as the pultrusion line speed.

2. The conservation equations are satisfied analytically. There is no transverse or longitudinal variations of volume fraction for the resin (V_f = const).

3. The contraction ratio of the die, λ=0.98, close to unity, is used in this study. This is a necessary geometry to obtain a complete analytical closed form solution for the flow field inside the die due to the mildly tapered geometry which is, however, negligibly small.

4. Unlike epoxy and polyester matrix resin, the impregnated resin matrix used in the current investigation is thermoplastic in nature with Newtonian properties. There is no chemical reactions occurring during the processing. Pressurizations due to thermal expansion, vaporization and shrinkage of the curing resin inside the die (commonly occurred for the thermosetting resin system) are absent.

5. The process is isothermal and in a steady state. Heat transfer is neglected, i.e., there is no temperature gradient inside the die and the resin matrix has a uniform viscosity [7].

6. The one directional permeability assumption in the main die section is characterized by the following relation (see also Fig. 2.1)

$$k_z(z) = \frac{D_f}{16Sz}\frac{(1 - V_f(z))^3}{V_f(z)^2} \tag{2.18}$$

where

$$h(z) = \lambda z + 1 - z \tag{2.19}$$

$$\frac{A(0)}{A(z)} = \frac{1}{[\lambda z + 1 - z]^2} \tag{2.20}$$

$$\begin{aligned} V_f(z) &= V_f(0)\left[\frac{A(0)}{A(z)}\right] \\ &= V_f(0)\frac{1}{[\lambda z + 1 - z]^2} \end{aligned} \tag{2.21}$$

$$\frac{k_z(z)}{k_z(0)} = \left[\frac{V_f(0)}{V_f(z)}\right]^2 \left[\frac{1 - V_f(z)}{1 - V_f(0)}\right]^3 \tag{2.22}$$

By knowing values of $V_f(0)$(or $k_z(0)$), one can calculate $k_z(z)$ at any z along the main die by Eqs. (2.21) and (2.22). The permeability for the unidirectional fiber structure exhibits anisotropic properties. For simplicity, the permeability of isotropic material is considered as constant, coincidently with the assumption 2.

7. Following dimensionless terms are defined:

$\underline{r} = r/R, \underline{z} = z/L, \underline{k} = k/R^2, \underline{v} = v/v_f, \underline{P} = PR^2/(\mu L v_f)$,

$\underline{f}(r) = f(r)/(v_f/L), \underline{h} = h/R = 1 - \underline{z}(1 - \lambda)$

2.3.2 Governing Equations and Boundary Conditions

An empirically modified Darcy's law suggested by Brinkman [8, 9] together with the condition of incompressibility for the flow through porous media is:

$$\vec{v} - k\nabla^2\vec{v} = -\frac{k}{\mu}(\nabla P) \tag{2.23}$$

$$\nabla \cdot \vec{v} = 0 \tag{2.24}$$

When the additional term with Laplace operator is dropped, Eq. (2.23) resembles the Darcy's law. An obvious difficulty of using the ordinary Darcy's law in calculations of flow problem is that the viscous shearing stresses acting on a volume element of fluid have been neglected; only the damping force of the porous mass has been retained. Hence the ordinary Darcy's law cannot be used as such in detailed flow analysis. Equation (2.23) with the inclusion of viscous stress tensor term has the advantage of approximating the ordinary Darcy's law for low values of k. When the values of k are high, it approximates the Navier Stokes equation for the viscous flow in empty space. The additional term with Laplace operator in Eq. (2.23) was intended to account for distortion of the velocity profiles near die walls. Unlike the ordinary Darcy's law, when Eqs. (2.23) and (2.24) are applied to flow through a porous medium in a tube, the result can be simplified to the Hagen-Poiseuille law when k approaches infinite [10].

Because of the assumption of small taper for the main pultrusion die, i.e., $\lambda = 0.98$, we may assume that $v_z = v_z(z,r)$, $v_r = v_r(r)$, $v_\theta = 0$ and $P = P(z)$. Consequently, Eqs. (2.23) and (2.24) become

$$v_z - k_z\left[\frac{1}{r}\frac{\partial}{\partial r}\left(r\frac{\partial v_z}{\partial r}\right) + \frac{\partial^2 v_z}{\partial z^2}\right] = -\frac{k_z}{\mu}\frac{dP}{dz} \tag{2.25}$$

$$v_r - k_r\left[\frac{1}{r}\frac{d}{dr}\left(r\frac{dv_r}{dr}\right)\right] = 0 \tag{2.26}$$

$$\frac{1}{r}\frac{d}{dr}(rv_r) + \frac{\partial v_z}{\partial z} = 0 \tag{2.27}$$

Note that the secondary flow, $v_r(r)$, is assumed to be a function of r only. From Eq. (2.27), it is obtained that $v_z(z,r) = zf(r) + v_f$, and $\partial^2 v_z/\partial z^2 = 0$ and, therefore, Eq. (2.25) becomes

$$\frac{df^2}{dr^2} + \frac{1}{r}\frac{df}{dr} - \frac{1}{k}f = \frac{dP}{z\mu \cdot dz} + \frac{v_f}{zk} \quad \text{(dimensional)} \tag{2.28}$$

Equation (2.28) is a dimensional form where the permeability in z-direction is denoted by $k = k_z = k_z(0)$, which was obtainable from flow analysis conducted earlier for the tapered section near the die entrance. Using the definitions of dimensionless terms, the dimensionless form of Eq. (2.28) with the underscore bars neglected is expressed as

$$\frac{d^2f}{dr^2} + \frac{1}{r}\frac{df}{dr} - \frac{1}{k}f = \frac{1}{z}\left(\frac{dP}{dz} + \frac{1}{k}\right) = C_0 \quad \text{(dimensionless)} \tag{2.29}$$

where C_0 is a constant. Equation (2.29) has the form of the modified Bessel's equation for f(r) with $n = 0$, $\alpha = K^{-1/2}$(see Appendix A).

2.3.3 The General Solution in the Dimensionless Form

A general solution of Eq. (2.29) is readily available as [11]

$$f(r) = C_1 I_0\left(\frac{r}{\sqrt{k}}\right) + C_2 K_0\left(\frac{r}{\sqrt{k}}\right) - kC_0 \tag{2.30}$$

The dimensionless boundary conditions are specified as

$$r = 0,\ df/dr = 0,$$

$$r = h,\ f = f(h) = -1/z$$

Thus, the complete (dimensionless) solution of Eq. (2.29) is found be

$$f(r) = \frac{1}{z}(v_z(z,r) - 1) = \left[kC_0 - \frac{1}{z}\right]\left[\frac{I_0\left(\frac{r}{\sqrt{k}}\right)}{I_0\left(\frac{h}{\sqrt{k}}\right)}\right] - kC_0 \tag{2.31}$$

Consequently, the velocity distribution inside the main pultrusion die section is expressed as

$$v_z(z,r) = [1 - zkC_0]\left[1 - \frac{I_0\left(\frac{r}{\sqrt{k}}\right)}{I_0\left(\frac{h}{\sqrt{k}}\right)}\right] \tag{2.32}$$

which satisfies the following boundary conditions

$$r = 0,\ dv_z/dr = 0,$$

$$r = h,\ v_z(z,h) = 0$$

Note that $v_z(0,0) = 1-1/Io(1/k^{1/2})$ approximates 1 (or in dimensional form $v_z(0)$ approximates v_f) from Eq. (2.32). Because of the small taper of the die, the secondary flow $v_r(r)$ is expected to be negligibly insignificant.

From Eq. (2.29), we have

$$\frac{dP}{dz} + \frac{1}{k} = C_0\, z \tag{2.33}$$

The value of constant C_0 is found to be

$$C_0 = 2\left[\frac{1}{k} - P_{en}(0)\right] \tag{2.34}$$

Solution of Eq. (2.33) is a parabolic function, and it is expressed as

$$P(z) = \left[\frac{1}{k} - P_{en}(0)\right]z^2 - \frac{1}{k}z + P_{en}(0) \tag{2.35}$$

This satisfies the boundary conditions: $P(z) = P_{en}(0)$ at $z = 0$ and $P(z) = 0$ at $z = 1$, where $P_{en}(0)$ is the pressure at the end of the tapered section near the die entrance, as calculated before. The pressure distribution is inversely proportional to the permeability k. Substituting Eq. (2.34) into Eq. (2.32), we have

$$v_z(z,r) = \{1 - 2[1 - kP_{en}(0)z]\}\left[1 - \frac{I_0\left(\frac{r}{\sqrt{k}}\right)}{I_0\left(\frac{h}{\sqrt{k}}\right)}\right] \tag{2.36}$$

where the dimensionless $h = 1-z(1-\lambda)$.

2.3.4 Discussion

Figure 2.4 shows the pultrusion die pressure distribution, Eq. (2.35), for various values of $P_{en}(0)$ indicated with $k = 9.19\times10^{-6}$. From Eqs. (2.33) and(2.34), we have

$$\frac{dP}{dz} = 2\left[\frac{1}{k} - P_{en}(0)\right]z - \frac{1}{k} \tag{2.37}$$

It is noted that at $z = 0$, dP/dz is negative, and other cases are discussed as follows:

Condition (i): $P_{en}(0) = 0$, then $0 < dP/dz = 1/k$ at $z = 1$. In this case, a minimum pressure occurs within the pultrusion die at $z_{min} = 1/2$.

Condition (ii): $dP/dz > 0$ or $0 < P_{en}(0) < 1/2k$ at $z = 1$. In this case, the minimum pressure occurs within the pultrusion die with

$$z_{min} = \frac{1}{2[1 - kP_{en}(0)]} \tag{2.38}$$

where $1/2 > z_{min} > 1.0$. Such a behavior of conditions (i) and (ii) was not observed experimentally for the pultrusion process.

In order to describe a pressure distribution with physical meaning, it is required to present other cases decribed below.

Condition (iii): $dP/dz \geq 0$ or $1/2k \leq P_{en}(0)$ at $z = 1$. In this case, the minimum pressure occurs at (when $P_{en}(0) = 1/2k$) or beyond (when $P_{en}(0) > 1/2k$) the die exit ($z = 1.0$).

Condition (iv): For $r = 0$ and any given $z = z_k$ along the die, Eq. (2.36) gives

$$v_z(z_k, 0) = \{1 - 2[1 - kP_{en}(0)]z_k\}\left[1 - \frac{1}{I_0\left(\frac{h_k}{\sqrt{k}}\right)}\right] \tag{2.39}$$

It is seen that in order to have $V_z(z_k) \geq V_z(0, 0)$ for any $z_k \geq 0$, one must have $P_{en}(0) \geq 1/k$. Consequently, we note that *$P_{en}(0) \geq 1/k$ is a necessary condition to obtain pressure and velocity distributions in a pultrusion die with physical significance.*

From the set of typical values for the pultrusion process given in Table 2.2, the pressure and velocity profiles can be calculated. The change of permeability along the pultrusion die is shown in Fig. 2.5. Values of k decrease dramatically in the entrance section of the die as a result of fast rise in fiber volume fraction, $V_f(z)$, shown in Fig. 2.2. It remains relatively unchanged within the main die section. The pressure profile in main die section is shown in Fig. 2.4. The pressure builts up quickly in the tapered section of the die within short length (α = 0.1), then decreases monotonically, with increasing negative slopes, and eventually vanishes at the die exit shown in Fig. 2.6. In the present example, it is noted that $P_{en}(0)=1.8\times10^{7}$ and $k=3.39\times10^{-7}$, and this results into $P_{en}(0)\times k=6.1$ which is greater than 1. Velocity distributions in three cross sections (z = 0.2, 0.5, 0.8) along the main die are shown in Figs. (2.7–2.9). The velocity profiles closely resemble the plug flows, i.e., the profiles are rather flat except in the narrow regimes near the die wall. It is noted that the velocities at the flat portions of the profiles are all higher than the fiber pulling speed, $v_f=5.08\times10^{-3}$ m/sec.

Substituting Eq. (2.36) into Eq. (2.27), the velocity $v_r(r)$ at any given location z along the main section of the pultrusion die can be obtained by integration as

$$v_r(r) = [1 - kP_{en}(0)]r - 2\sqrt{k}[1 - kP_{en}(0)]\{\frac{I_1\left(\frac{r}{\sqrt{k}}\right)}{I_0\left(\frac{h_k}{\sqrt{k}}\right)}\}+$$

$$(1 - \lambda)\{1 - 2[1 - kP_{en}(0)]z_k\}\{\frac{I_1\left(\frac{h_k}{\sqrt{k}}\right)I_1\left(\frac{r}{\sqrt{k}}\right)}{\left[Io\left(\frac{h_k}{\sqrt{k}}\right)\right]^2}\} \qquad (2.40)$$

which satisfies the boundary condition of $v_r(0)$ along the pultrusion die. The velocity $v_r(r)$ at any given $z = z_k$ and $h_k = 1-z_k(1-\lambda)$ can be shown to be negligibly small when compared with $v_z(z_k, r)$.

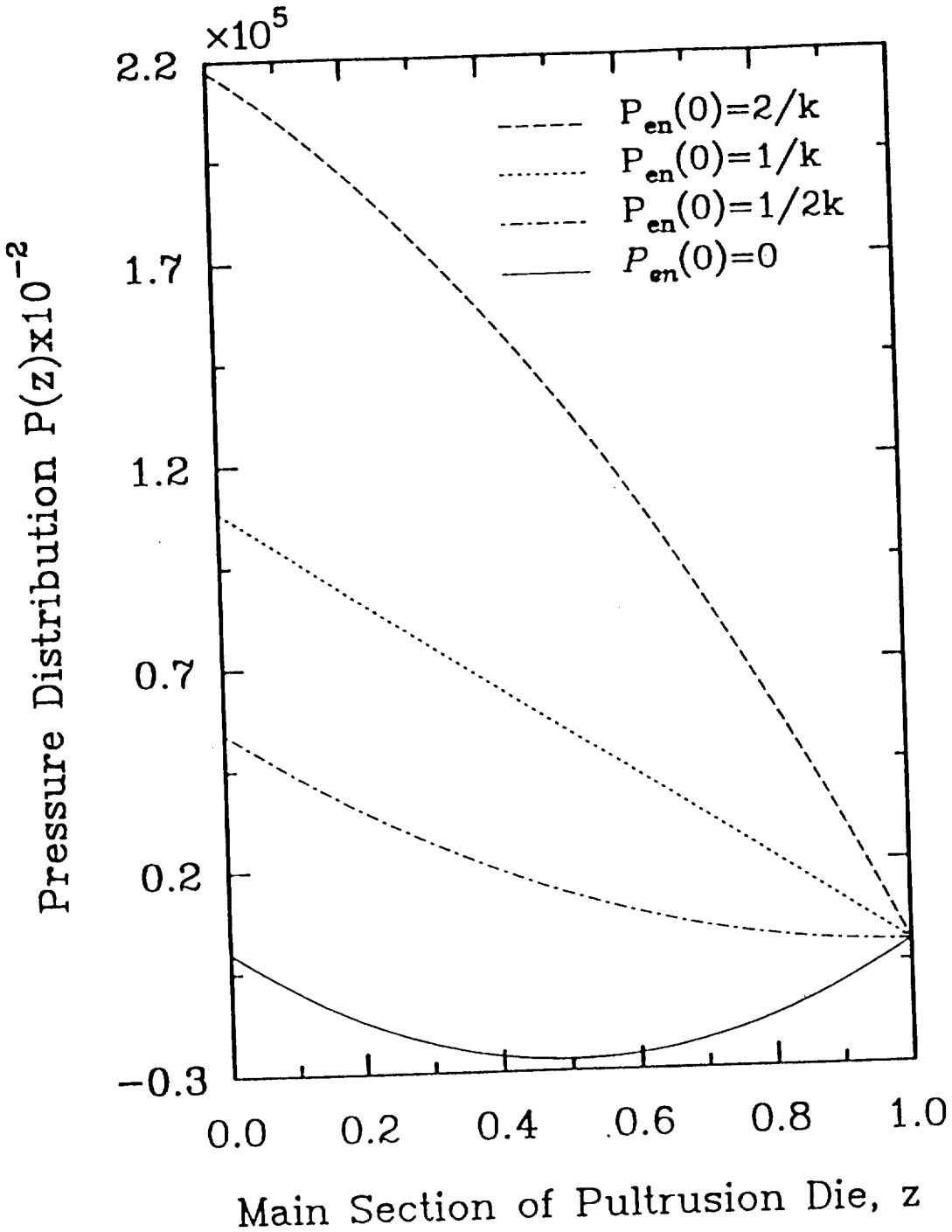

Fig. 2.4 Pressure Distribution in the Main Die; α=0.1, ϵ=1.5, V_o=0.1 and k=9.19×10^{-6}.

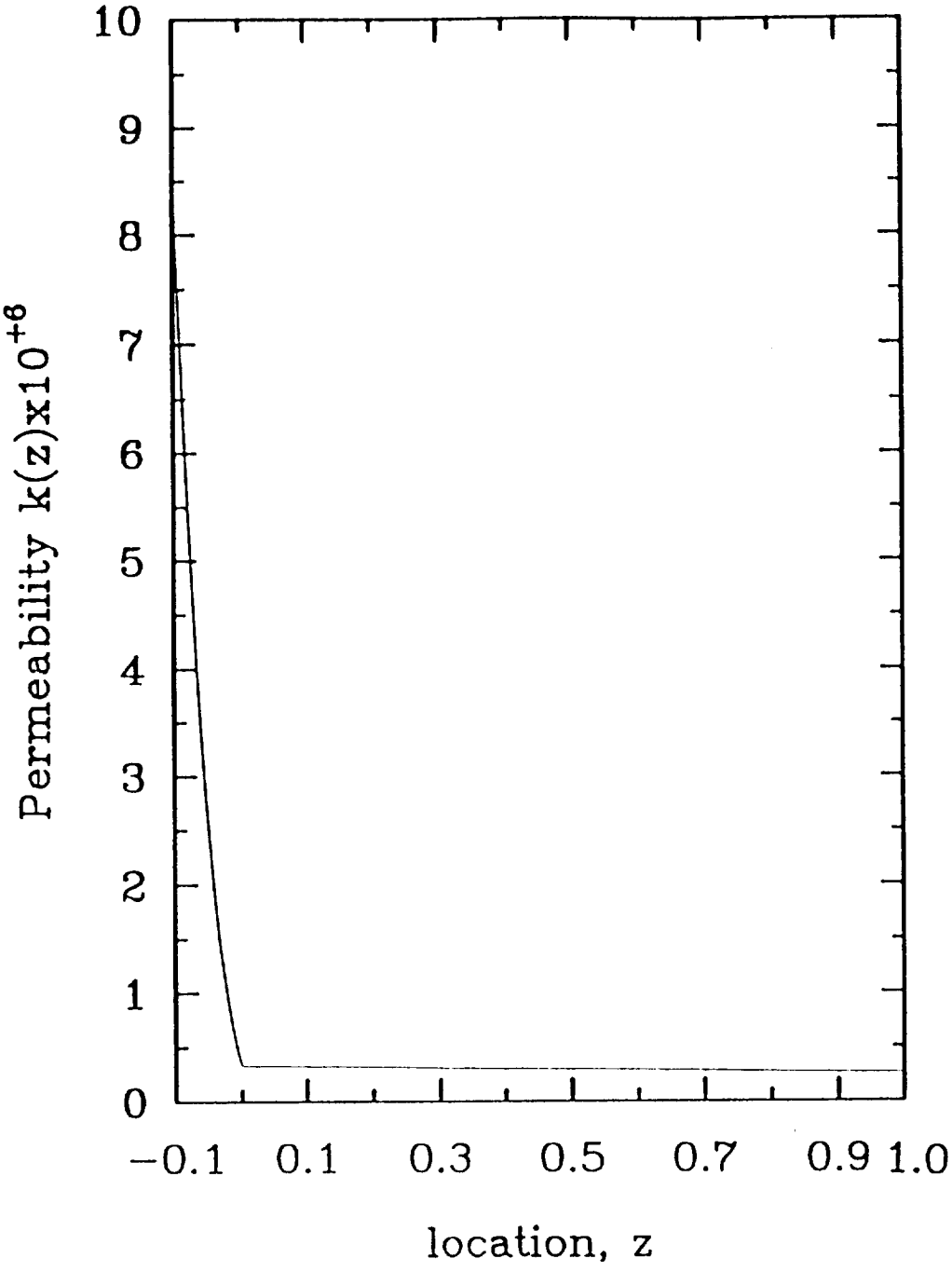

Fig. 2.5 Change Permeability along the Pultrusion Die; α=0.1, ϵ=1.5, V_o=0.25, λ=0.98, D_f=0.002 and S_z=1.

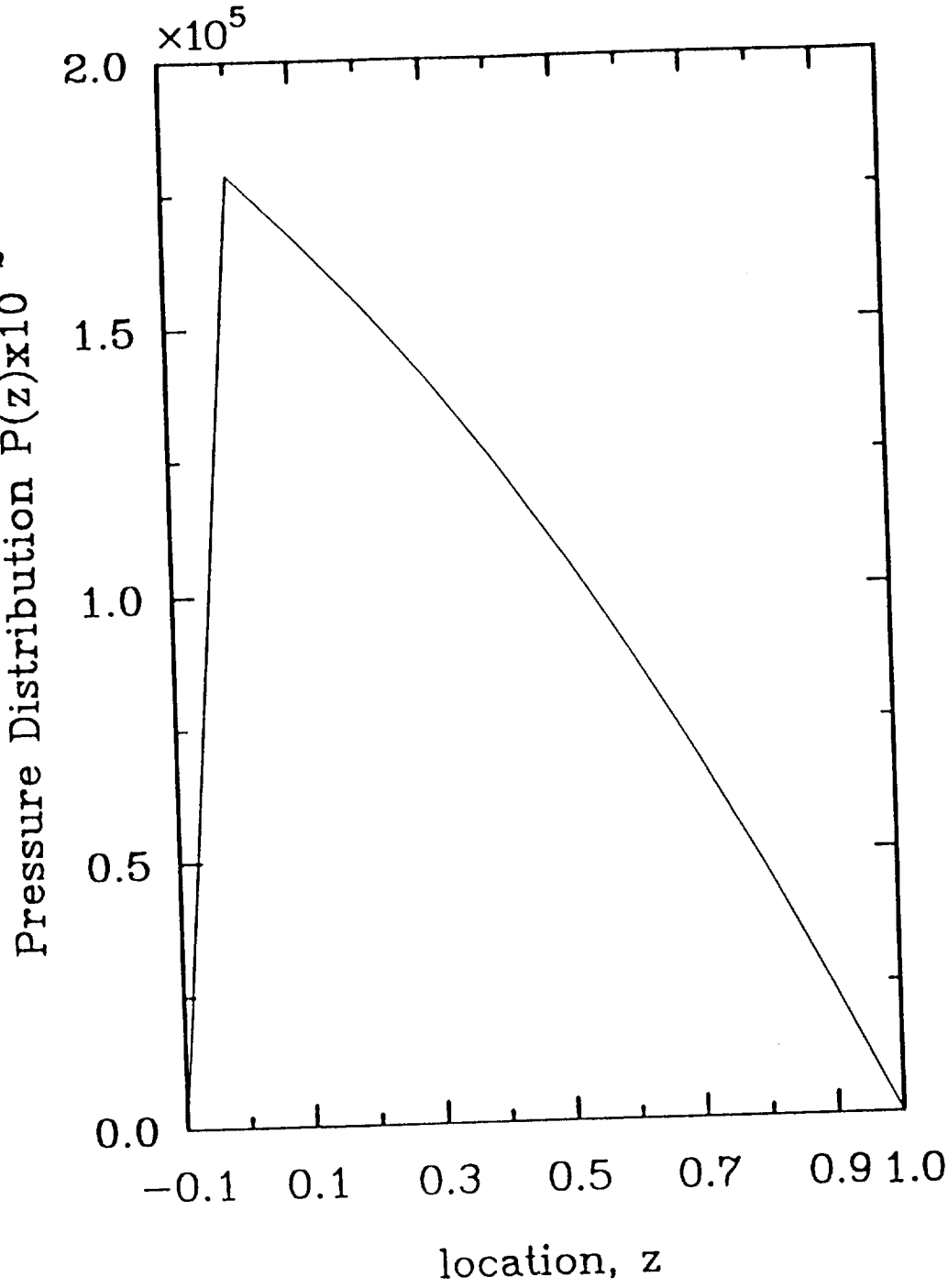

Fig. 2.6 Pressure Distribution; α=0.1, ϵ=1.5, V_o=0.25, ΔT=200°C, D_f=0.002, S_z=1, $\alpha_v=5\times10^{-5}$ °C^{-1}, $\kappa_c=5\times10^{-10}$m^{2}N^{-1}, μ=0.14P_aS_{ec}, R=6.35×10^{-3}m, L=0.3048m and $v_f=6.35\times10^{-3}$m/sec.

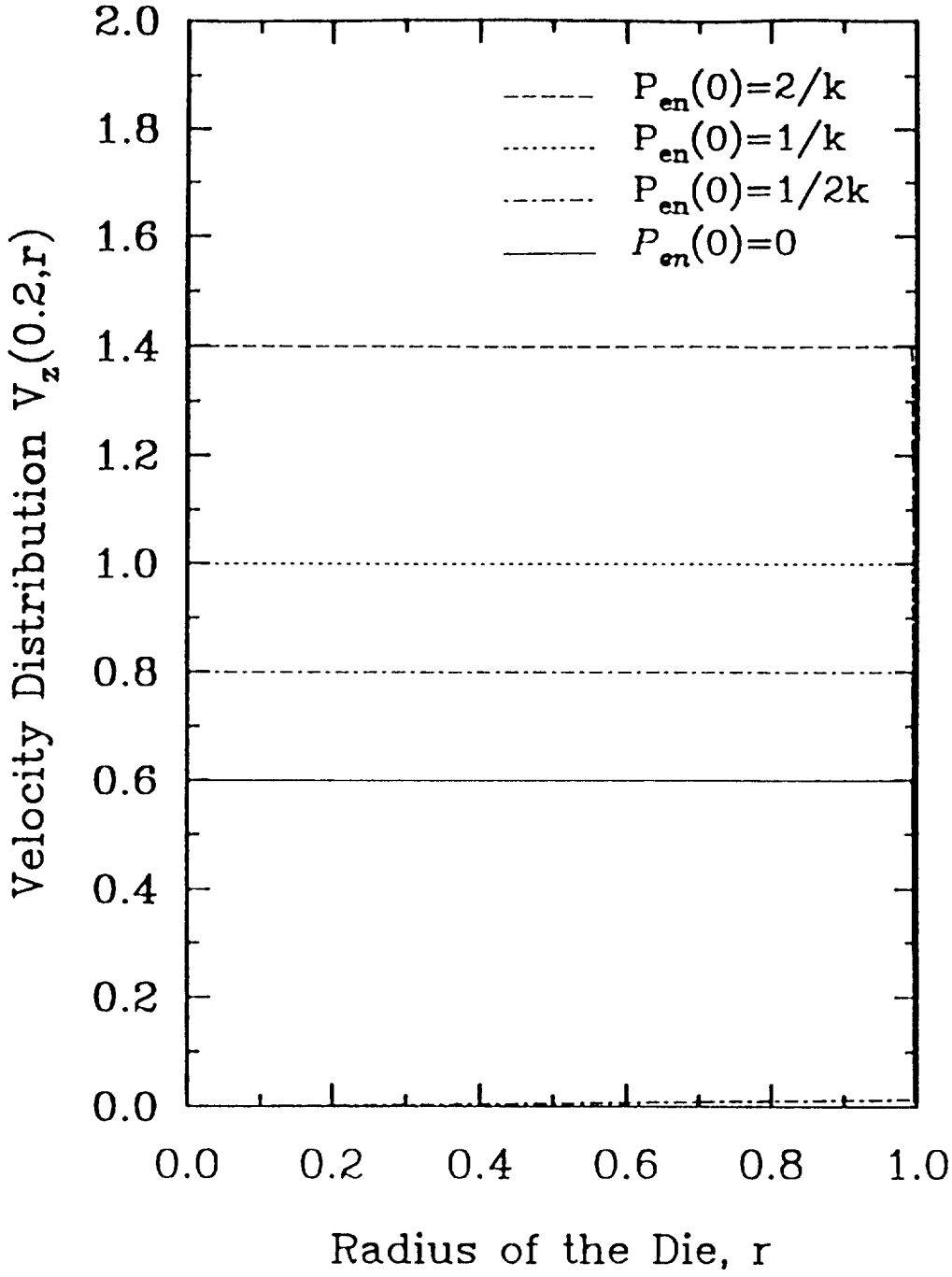

Fig. 2.7 Velocity Vs Radius at Location z=0.2; k=3.39×10^{-7}.

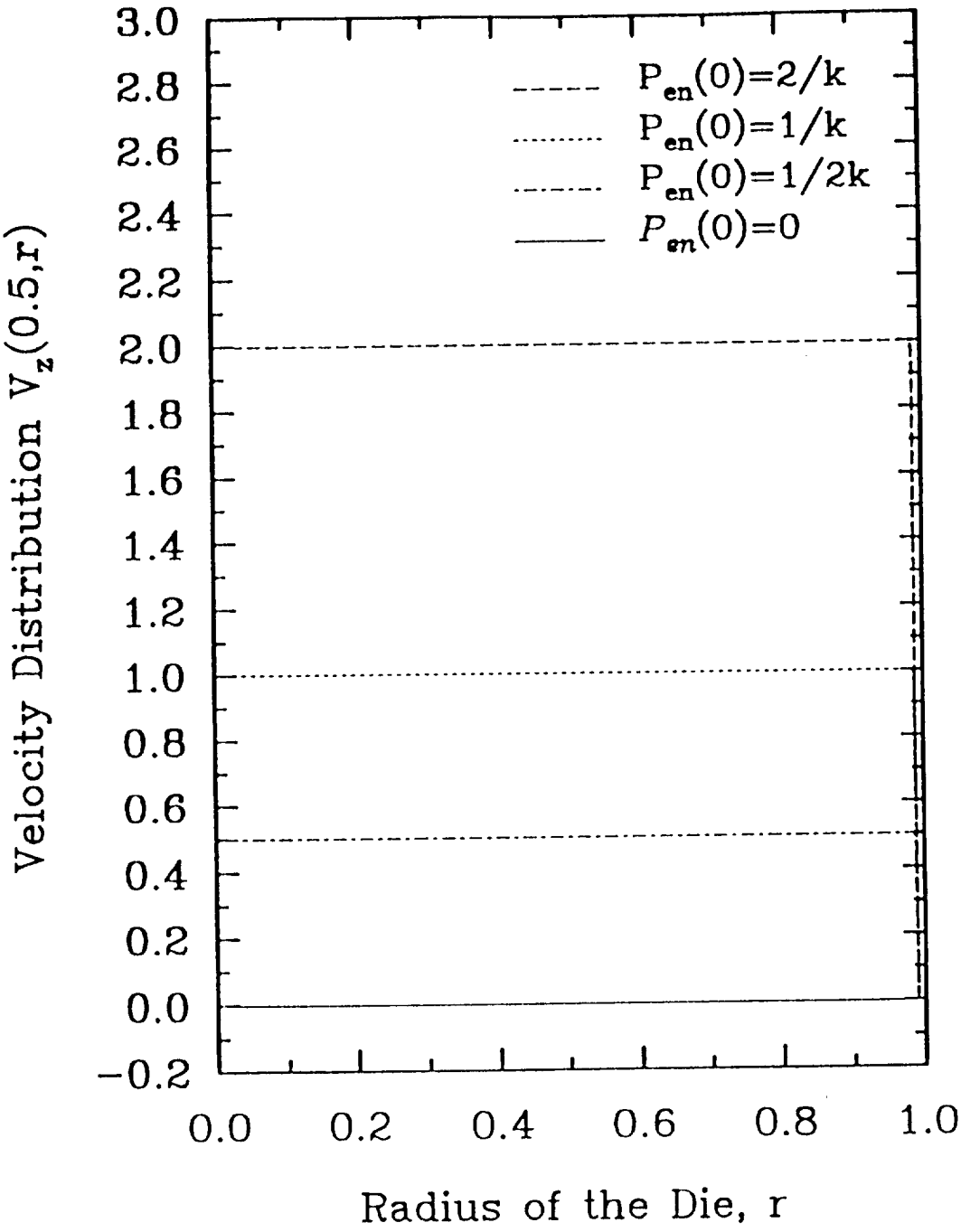

Fig. 2.8 Velocity Vs Radius at Location z=0.5; $k=3.39\times10^{-7}$.

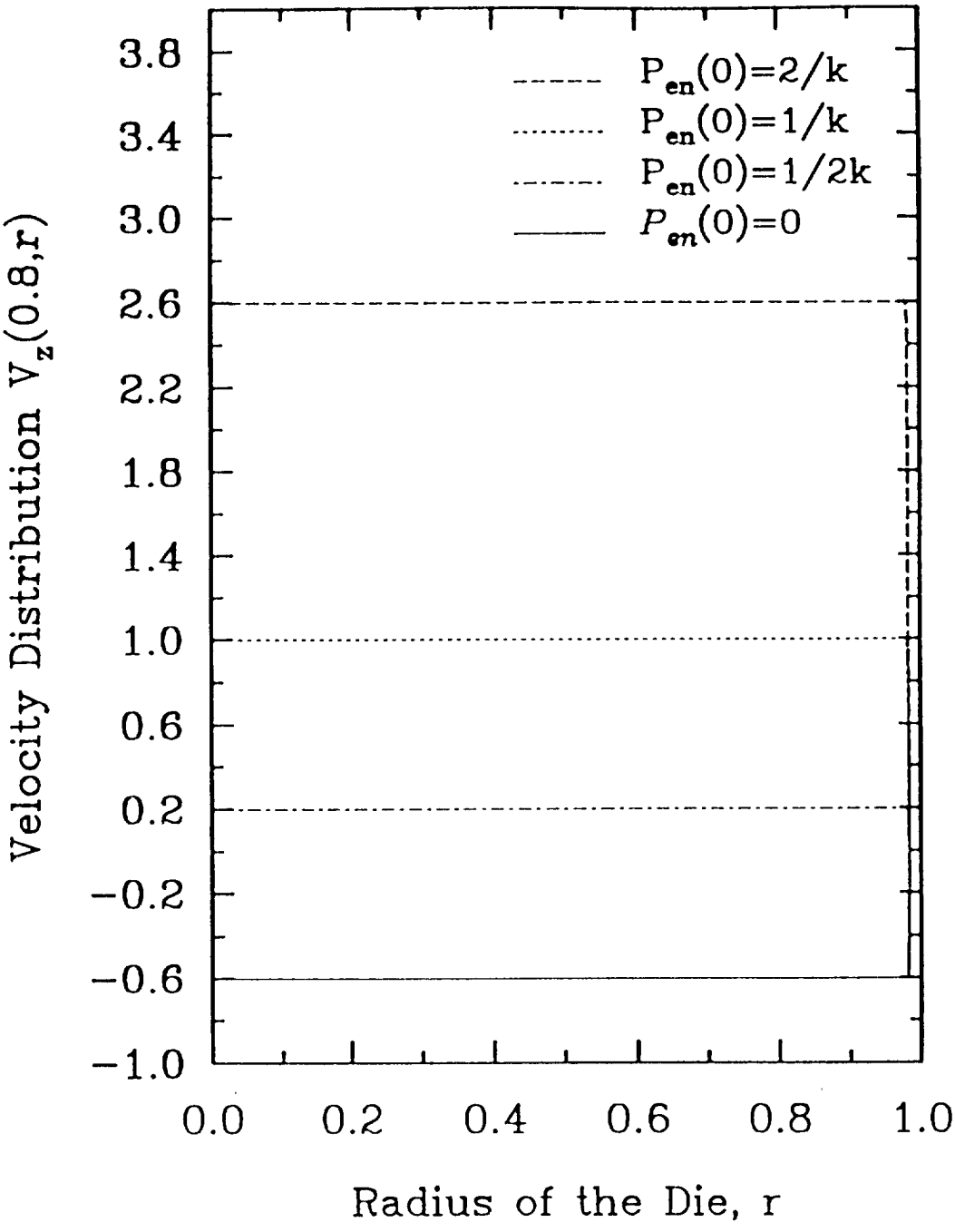

Fig. 2.9 Velocity Vs Radius at Location z=0.8; $k=3.39\times10^{-7}$.

Chapter 3

ANALYSIS OF PULLING FORCES

3.1 Calculation of the Pulling Force

Forces generated in a die are functions of stock velocity, reinforcing configuration, resin system and pultruding conditions, materials, etc. They are summarized below according to the acting effects:

(a) Frictional forces (fiber friction against the die wall).

(b) Viscous forces (shear viscous flow in a thin layer).

(c) Collimation forces (backflow drag resistance on fibers, fiber compact).

(d) Temperture-induced forces (increasing viscosity and resin thermal expansion).

Following dimensionless force terms are defined :

$$\underline{F}_v = F_v/(\mu L v_f), \underline{F}_f^I = F_f^I/(\mu L v_f), \underline{F}_f^{II} = F_f^{II}/(\mu L v_f), \underline{F}_f^{III} = F_f^{III}/(R^2 L K_{FENEC})$$

$$\underline{P} = PR^2/(\mu L v_f), \underline{P}_{fe} = P_{fe}/(K_{FENEC} R), \underline{\tilde{K}}_{FENEC} = K_{FENEC} R^2/(\mu v_f)$$

$$\underline{\tilde{F}}_f^{III} = \underline{F}_f^{III}\underline{\tilde{K}}_{FENEC}, \underline{\tilde{P}}_{fe} = \underline{P}_{fe}\underline{\tilde{K}}_{FENEC}, \underline{F}_c^c = F_c^c/(R^2 L K_{FENEC})$$

$$\underline{\tilde{F}}_c^c = \underline{F}_c^c\underline{\tilde{K}}_{FENEC}, \underline{F}_c^b = F_c^b/(\mu L v_f), \underline{F}_c^k = F_c^k/(\mu L v_f)$$

$$\underline{h}(z) = h(z)/R, \underline{h}(-\alpha) = \underline{h}(-\alpha)/R = \epsilon, \underline{h}(\infty) = \underline{h}(\infty)/R$$

where $\left(F_f^{III}\right)_M$, $\left(F_f^{III}\right)_T$ and $\left(F_c^c\right)_T$ are written without tilde in Table 3.1.

Table 3.1 Category of Pulling Force

Types of Contribution	Sources of Contribution	Tapered Entrance	Main Die Section	Summation
Viscous Force F_v	1. Shear Flow		$(F_v)_M$	$F_v = (F_v)_M$
Friction Force F_f	1. Hydrostatic Pressure 2. Normal Stress 3. Fiber Compaction	$(F_f^{III})_T$	$(F_f^{I})_M$ $(F_f^{II})_M$ $(F_f^{III})_M$	$F_f = (F_f^{I})_M + (F_f^{II})_M + (F_f^{III})_M + (F_f^{III})_T$
Collimation Forces F_c	1. Bulk 2. Compaction Back Flow 3. Thermal Expansion	$(F_c^{c})_T$ $(F_c^{b})_T$ $(F_c^{k})_T$	$(F^{k}_{c})_M$	$F_c = (F_c^{c})_T + (F_c^{b})_T + (F_c^{k})_T + (F_c^{k})_M$

3.1.1 Viscous Drag Force Contribution, F_v

We first consider the viscous drag contribution in the entire pultrusion die $-\alpha L \le z \le L$. This is expressed as

$$F_v = \int_{-\alpha L}^{L} \tau_{rz}]_{r=h}\ 2\pi h\, dz$$

$$= \int_{-\alpha L}^{0} \left(-\mu \frac{dV_z}{dr}\right)_{r=h} 2\pi h\, dz +$$

$$\int_{0}^{L} \left(-\mu \frac{dV_z}{dr}\right)_{r=h} 2\pi h\, dz \qquad \text{(dimensional)} \tag{3.1}$$

The first integration of Eq. (3.1) between the length ($-\alpha L \le z \le L$) is equal to zero because of the "plug flow" assumption made in the entrance tapered section. This may not be serious assumption. Using the dimensionless terms defined above without the underscore bar, and noting the dimensionless relationships of the main die section geometry $h = 1 - z(1-\lambda), dh = -(1-\lambda)dz$, we have

$$F_v = 2\pi \int_{0}^{1} h\left[-\frac{dV_z}{dr}\right]_{r=h} dz = \left(\frac{2\pi}{1-\lambda}\right) \int_{1}^{\lambda} h\left[\frac{dV_z}{dr}\right]_{r=h} dh$$

$$= \left(\frac{2\pi}{1-\lambda}\right) \int_{1}^{\lambda} -\frac{1}{\sqrt{k}} \left\{1 - 2[1 - kP_{en}(0)]\left[\frac{1-h}{1-\lambda}\right]\right\} \left[\frac{hI_1\left(\frac{h}{\sqrt{k}}\right)}{I_0\left(\frac{h}{\sqrt{k}}\right)}\right] dh \tag{3.2}$$

Equation (3.2) is the contribution of viscous drag force from the main die section to the total pultrusion force. It is noted that F_v is a function of permeability k and $kP_{en}(0)$ only for a given die geometry and pultruded prepreg system; the results are shown in Fig. 3.1.

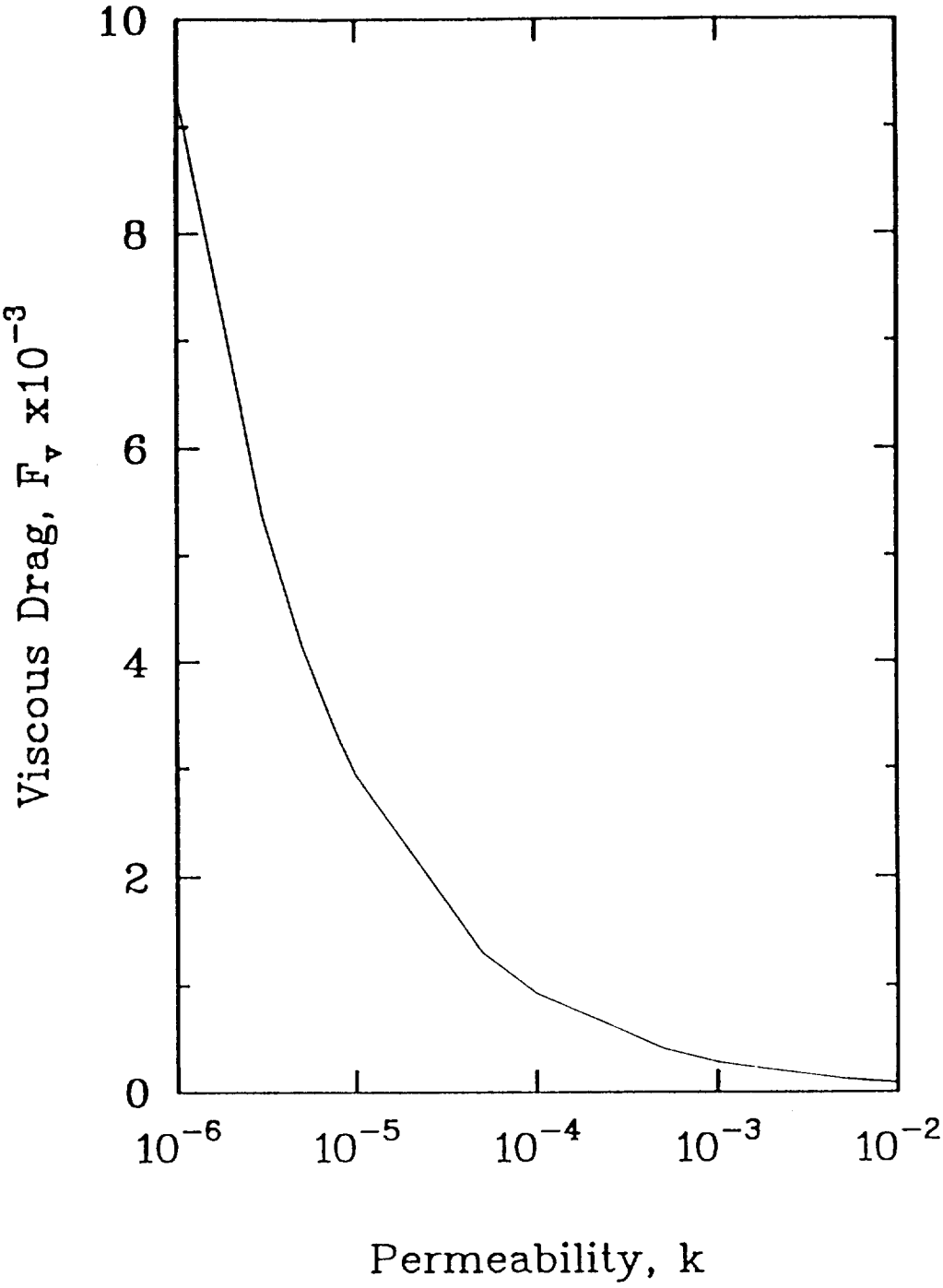

Fig. 3.1 Viscous Drag Force Vs Permeability; $kP_{en}(0)=1.5$ and $\lambda=0.98$.

3.1.2 Friction Force Contribution, F_f

The friction force is originated solely from the relative movement between fiber bundles and the die wall, and is the product of the frictional coefficient (μ_f) and the normal forces acting on the wall surfaces. The normal forces acting on the wall surfaces have four sources of contribution: (I) the hydrostatic pressure, (II) the normal stress generated by the flow inside the pultrusion die, (III) the fiber compaction forces due to the contraction geometry of the die, and (IV) the vaporization and shrinkage forces due to chemical curing reactions of resin system. In the present investigation we deal with the thermoplastic materials, effect due to the reactions do not exist in our consideration. The other three sources of contribution to the friction force are presented below.

3.1.2.1 Hydrostatic Pressure Contribution, F_f^I From the information on area, normal force, and frictional coefficient, μ_f, the relation for F_f^I is expressed as

$$F_f^I = 2\pi\mu_f \int_{-\alpha L}^{L} P(z)\, h(z)\, dz \quad \text{(dimensional)} \tag{3.3}$$

Since a "plug flow" assumption with a uniform velocity $v_z(z,r) = v_f$ was made in the tapered die section, there is no pressure gradient along length ($-\alpha L \le z \le 0$). Therefore Eq. (3.3) is simplified as

$$F_f^I = \left(F_f^I\right)_M = 2\pi\mu_f \int_{0}^{L} P(z)\, h(z)\, dz \quad \text{(dimensional)} \tag{3.4}$$

With the dimensionless forms for all parameters difined earlier, the dimensionless expression for Eq. (3.4) without the underscore bar is as follows:

$$F_f^I = 2\pi\mu_f \int_{0}^{1} \left(\frac{L}{R}\right) P(z)\, h(z)\, dz \tag{3.5}$$

where $h = 1 - z(1-\lambda)$, $0 \le z \le 1$ and

$$P(z) = \left[\frac{1}{k} - P_{en}(0)\right] z^2 - \left(\frac{1}{k}\right) z + P_{en}(0) \tag{3.6}$$

Substituting Eq. (3.6) into Eq. (3.5) and performing the integration, we obtain a closed form solution as

$$F_f^I = \pi \left(\frac{L}{R}\right) \left(\frac{\mu_f}{k}\right) \left\{ -\frac{1+\lambda}{6} + kP_{en}(0) \left[\frac{5}{6} + \frac{\lambda}{2}\right] \right\} \tag{3.7}$$

It is noted that F_f^I is a function of k and $kP_{en}(0)$ only. The solution given by Eq. (3.7) is illustrated in Fig. 3.2. It is seen that F_f^I decrease continuously with increasing values of k.

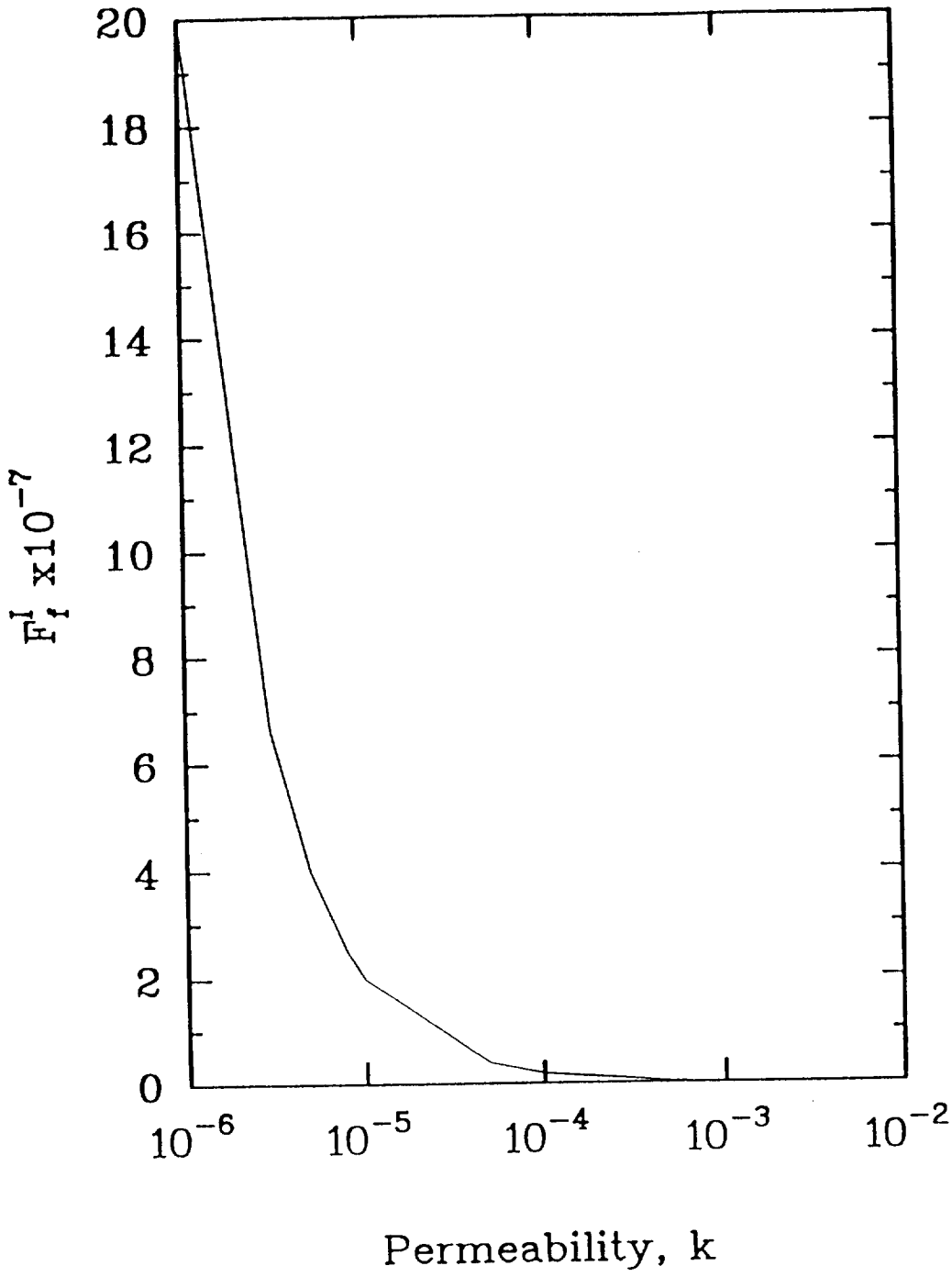

Fig. 3.2 Friction Force due to Hydrostatic Pressure, F_f^I Vs Permeability k; μ_f=0.8, λ=0.98, $kP_{en}(0)$=1.5, R=6.35×10^{-3}m and L=0.3048m.

3.1.2.2 Normal Stress Contribution, F_f^{II} For a given frictional coefficient, μ_f, the relation for F_f^{II} is given by

$$F_f^{II} = 2\pi\mu_f \int_{-\alpha L}^{L} \{\tau_{rr}\}_{r=h}\, h(z)\, dz \qquad \text{(dimensional)} \tag{3.8}$$

where $\tau_{rr} = -2\mu(\partial v_r/\partial r)$ for the Newtonian fluid is the normal stress in r-direction. From the continuity equation, Eq. (2.27), we have $\tau_{rr} = 2\mu(v_r/r + \partial v_z/\partial z)$. Again the "the plug flow" assumption with constant $v_z(z,r)$ and negligible v_r is used in the flow analysis of the tapered die section. Thus, Eq. (3.8) becomes

$$F_f^{II} = \left(F_f^{II}\right)_M = 2\pi\mu_f \int_{0}^{L} \{\tau_{rr}\}_{r=h}\, h(z)\, dz \quad \text{(dimensional)} \tag{3.9}$$

The dimensionless form of Eq. (3.9) without the underscore bar is given as

$$\begin{aligned} F_f^{II} &= 2\pi\mu_f \int_{0}^{1} \left\{2\left[\frac{V_r}{r} + \left(\frac{R}{L}\right)\frac{\partial V_z}{\partial z}\right]\right\}_{r=h} h(z)\, dh \\ &= -\left(\frac{1}{1-\lambda}\right)2\pi\mu_f \int_{1}^{\lambda} \left\{2\left[\frac{V_r}{r} + \left(\frac{R}{L}\right)\frac{\partial V_z}{\partial z}\right]\right\}_{r=h} h\, dh \end{aligned} \tag{3.10}$$

In the main pultrusion die section ($0 \le z \le 1$ or $\lambda \le h \le 1$), the secondary flow, $v_r(r)$, at the wall ($r = h$) is neglected. Consequently, we have

$$F_f^{II} = -\left(\frac{2\pi}{1-\lambda}\right)\mu_f \int_{1}^{\lambda} \left\{2\left(\frac{R}{L}\right)\frac{\partial V_z}{\partial z}\right\}_{r=h} h\, dh \tag{3.11}$$

where $h = 1 - z(1-\lambda)$, $0 \le z \le 1$ or $\lambda \le h \le 1$ and

$$\begin{aligned} \frac{\partial V_z}{\partial z}\Big]_{r=h} &= -(1-\lambda)\frac{\partial V_z}{\partial h}\Big]_{r=h} \\ &= -\frac{1}{\sqrt{k}}\{(1-\lambda) - 2[1 - kP_{en}(0)](1-h)\}\left[\frac{I_1\left(\frac{h}{\sqrt{k}}\right)}{I_0\left(\frac{h}{\sqrt{k}}\right)}\right] \end{aligned} \tag{3.12}$$

A combination of Eqs. (3.11) and (3.12) results in

$$F_f^{II} = \frac{\mu_f}{\sqrt{k}}\left(\frac{4\pi}{1-\lambda}\right)\left(\frac{R}{L}\right)\int_1^{\lambda}\{(1-\lambda)-2[1-kP_{en}(0)](1-h)\}\left[\frac{I_1\left(\frac{h}{\sqrt{k}}\right)}{I_0\left(\frac{h}{\sqrt{k}}\right)}\right]h\,dh \quad (3.13)$$

It is noted that $F_f^{II}(k)$ is a function of k and $kP_{en}(0)$ only. The results of this equation are shown in Fig. 3.3.

3.1.2.3 Fiber Compaction Contribution, F_f^{III} A composite laminate pultruded through the die with a tapered entrance section is expected to experience continuous compaction in the lateral r-direction. The laminate could be viewed as a fiber bundle with multi-filament layers in which exists numerous points of contact among the individual filament layers. Any degree of compaction applied to the fiber bundle will raise the fiber volume fraction, and increase the fiber elastic forces. It was observed experimentally [12–15] that forces required to compact the fiber bundles increased dramatically when the fiber volume fraction, V_f, approached a limiting value of V_∞. Considering the fiber bundles as a whole an elastic spring, we proposed a phenomenological model for the fiber elastic force, F_e, based upon the Finitely Extendable Nonlinear Elastic (FENE) spring concept:

$$F_e(t) = K_{FENE}\left\{\frac{\hat{h}(0)-\hat{h}(t)}{\left[1-\left(\frac{\hat{h}(0)-\hat{h}(t)}{\hat{h}(0)-\hat{h}(\infty)}\right)\right]}\right\} \quad (3.14)$$

where $F_e(t)$ is the elastic force at $\hat{h}(t)$, and $\hat{h}(t)$ is the thickness of the fiber mat at t with $\hat{h}(0)$ denoting the initial thickness with no compaction occurred. The difference $\hat{h}(0)-\hat{h}(\infty)$ represents the maximum compaction achievable for a given fiber mat. This model has three adjustable parameters: n, $\hat{h}(\infty)$ and spring constant K_{FENE}. A fiber mat with this force law will behave as a linear (Hookean) spring for small compaction, but will get stiffer and stiffer (nonlinear behavior) as the compaction increased. Furthermore, the laminate cannot be compacted beyond $\hat{h}(\infty)$ (or in an other word, exceed $\hat{h}(0)-\hat{h}(\infty)$), because infinitely large compaction force will then be required according to Eq. (3.14).

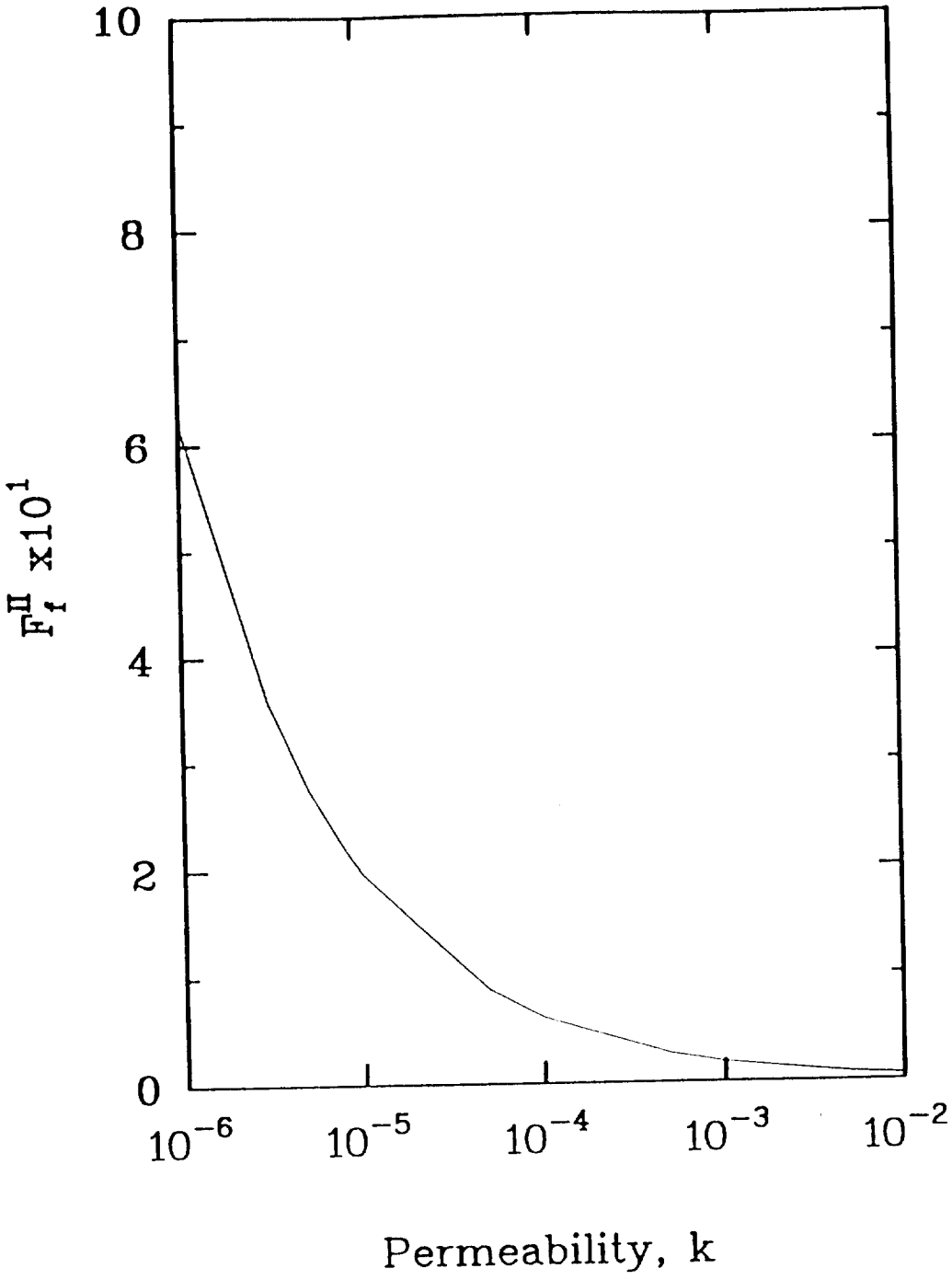

Fig. 3.3 Friction Force due to Normal Stress Contribution, F_f^{II} Vs Permeability k; μ_f=0.8, λ=0.98, $kP_{en}(0)$=1.5, R=6.35×10^{-3}m and L=0.3048m.

In the pultrusion process presently studied, total fiber volume remains constant throughout the pultrusion die of Fig. 2.1. The quantity $\hat{h}(z)$ in Eq. (3.14) will be the radius of the pultrusion die at z with $\hat{h}(0)$ denoting the radius of die entrance ($\hat{h}(0)$ = h(-α) = ϵ) where no compaction occurs. Then for a laminate rod pultruded through the tapered die, we have

$$P_{fe}(z) = K_{FENEC}\left\{\frac{\hat{h}(-\alpha) - \hat{h}(z)}{\left[1 - \left(\frac{\hat{h}(-\alpha)-\hat{h}(z)}{\hat{h}(-\alpha)-\hat{h}(\infty)}\right)\right]^{n}}\right\} \text{ (dimensional)} \tag{3.15}$$

where $P_{fe}(z)$ is the pressure acting on a characteristic surface of the die wall at z, and $K_{FENEC} = K_{FENE}/(\text{unit area})$ in the units of (force per(length)^3) is a material property determined experimentally for a given random fiber mat or aligned unidirctional prepreg system. The results of Eq. (3.15) are shown in Fig. 3.4. Using the dimensionless terms defined earlier, we have the dimensionless form of Eq. (3.15), with the underscore bars neglected, as

$$P_{fe}(z) = \left\{\frac{h(-\alpha) - h(z)}{\left[1 - \left(\frac{h(-\alpha)-h(z)}{h(-\alpha)-h(\infty)}\right)\right]^{n}}\right\} \tag{3.16}$$

with

$$h(z) = 1 - z\left(\frac{\epsilon - 1}{\alpha}\right), \quad -\alpha \le z \le 0 \tag{3.17}$$

$$h(z) = 1 - z(1 - \lambda), \quad o \le z \le 1 \tag{3.18}$$

There are no physical meanings attached to the parameters K_{FENEC} and n. However, it is reported that this model can describe the deformations of both random fiber mats and aligned prepreg fibers rather well with reasonable values of $V_0 = V_f(-\alpha), V_\infty = V_f(\infty)$. It is seen that this model is simple but adequate for meeting the objective of present study, and is used in the following discussion.

For a frictional coefficient, μf, we have fiber compaction to the total pulling force in a dimensional form as

$$F_f^{III} = 2\pi\mu_f \int_{-\alpha L}^{L} P_{fe}(z)\, h(z)\, dz \quad \text{(dimensional)} \tag{3.19}$$

The dimensionless form of Eq. (3.19) with underscore bar neglected is

$$\begin{aligned} F_f^{III} &= \left(F_f^{III}\right)_T + \left(F_f^{III}\right)_M \\ &= 2\pi\mu_f \int_{-\alpha}^{1} P_{fe}(z)\, h(z)\, dz \\ &= 2\pi\mu_f \int_{-\alpha}^{0} P_{fe}(z)\, h(z) \cos\phi\, dz + 2\pi\mu_f \int_{0}^{1} P_{fe}(z)\, h(z)\, dz \end{aligned} \tag{3.20}$$

In order to compare the magnitudes of various force contributions, additional dimensionless force, pressure and elastic spring constant are defined as: $\tilde{F}_f^{III}$, $\tilde{P}_{fe}$, $\tilde{K}_{FENEC}$, respectively. Then, neglecting the underscore bar, the new dimensionless form of Eq. (3.20) becomes:

$$\tilde{F}_f^{III} = 2\pi\mu_f \{ \int_{-\alpha}^{0} \tilde{P}_{fe}(z) \cos\phi dz + \int_{0}^{1} \tilde{P}_{fe}(z)\, h(z) dz \} \tag{3.21}$$

or

$$\begin{aligned} \tilde{F}_f^{III} = 2\pi\mu_f \tilde{K}_{FENEC} \{ &\left(-\frac{\alpha}{\epsilon - 1}\right) \int_{\epsilon}^{1} \{ \frac{\epsilon - h}{\left[1 - \left(\frac{\epsilon - h}{\epsilon - h(\infty)}\right)\right]^n} \} h \cos\phi dh \} \\ &+ \left(-\frac{1}{1-\lambda}\right) \int_{1}^{\lambda} \{ \frac{\epsilon - h}{\left[1 - \left(\frac{\epsilon - h}{\epsilon - h(\infty)}\right)\right]^n} \} h\, dh \end{aligned} \tag{3.22}$$

Equation (3.22) is obtained by means of Eqs. (3.17) and (3.18) and $\phi = \tan^{-1}[(\epsilon - 1)/\alpha]$. Because of the tapered geometry, the fiber volume fraction $V_f(z)$ is expected to increase along the die. As shown before for the cylindrical die ($-\alpha \le z \le 0$), we have

$$V_f(z) = V_0\left[\frac{A(-\alpha)}{A(z)}\right] = V_0\left[\frac{h(-\alpha)}{h(z)}\right]^2 \tag{3.23}$$

or

$$\frac{h(-\alpha)}{h(\infty)} = \sqrt{\frac{V_f(\infty)}{V_0}} \tag{3.24}$$

For an aligned prepreg system, n=1.5, $V_f(\infty)$ = 0.74 and $K_{FENE} = K_{FENEC}$ = 50 psi, were found for the FENE model (Eq.(3.14)) to describe elastic forces reasonably well. For R = 0.125 in, V_0 = 0.1 and h(-α) = ϵ = 1.5 from Table 2.2, values of K_{FENEC} = 400 lb in $^{-3}$ and $h(\infty)$ = 0.55 can be calculated.

Total contribution of the frictional forces to the pulling force is: $F_f = F_f^I + F_f^{II} + \tilde{F}_f^{III}$ given by Eqs. (3.7), (3.13) and (3.22). The comparison among frictional forces is shown in Fig. 3.5.

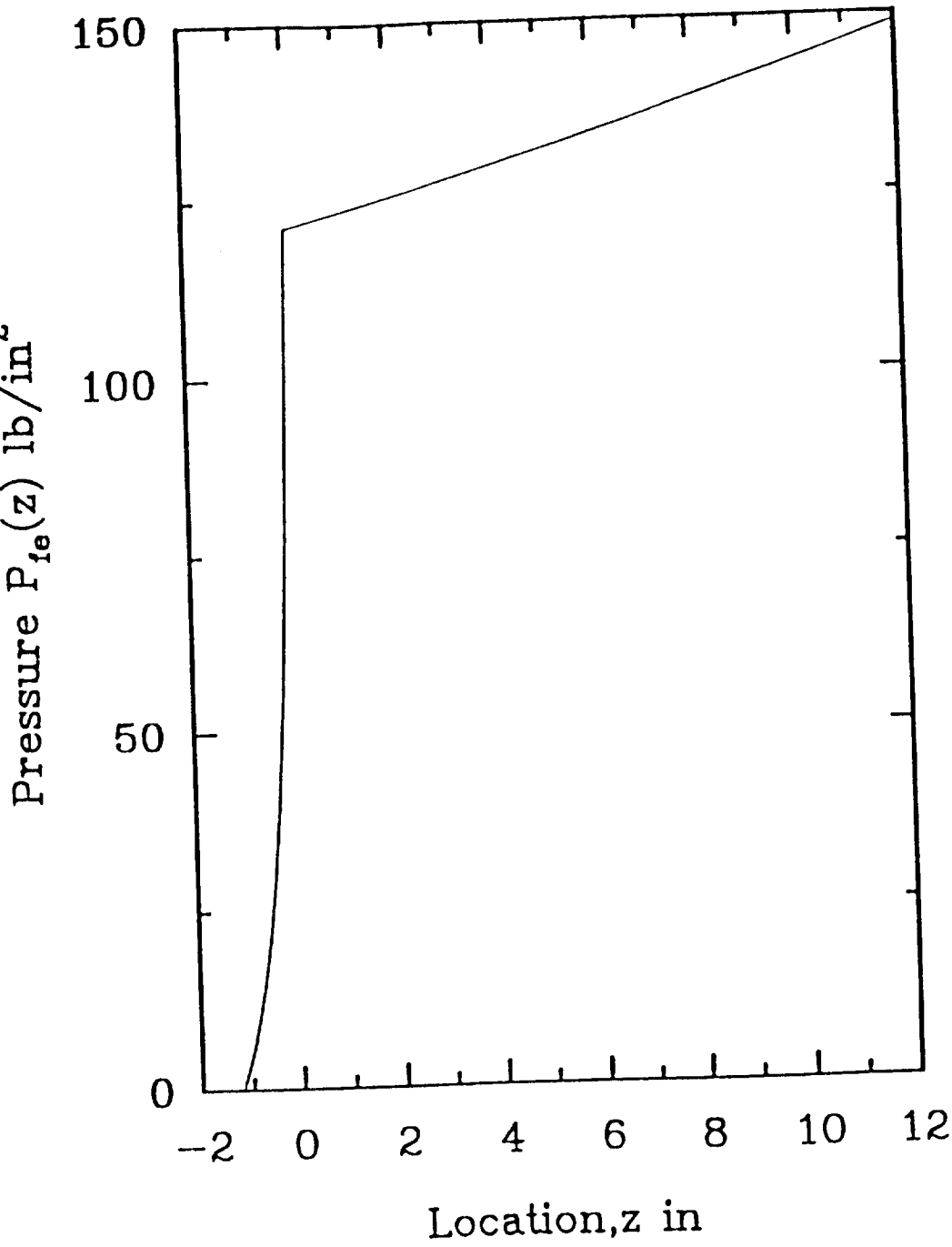

Fig. 3.4 Pressure $P_{fe}(z)$ based on the FENE Spring Concept; α=0.1, ϵ=1.5 and λ=0.98.

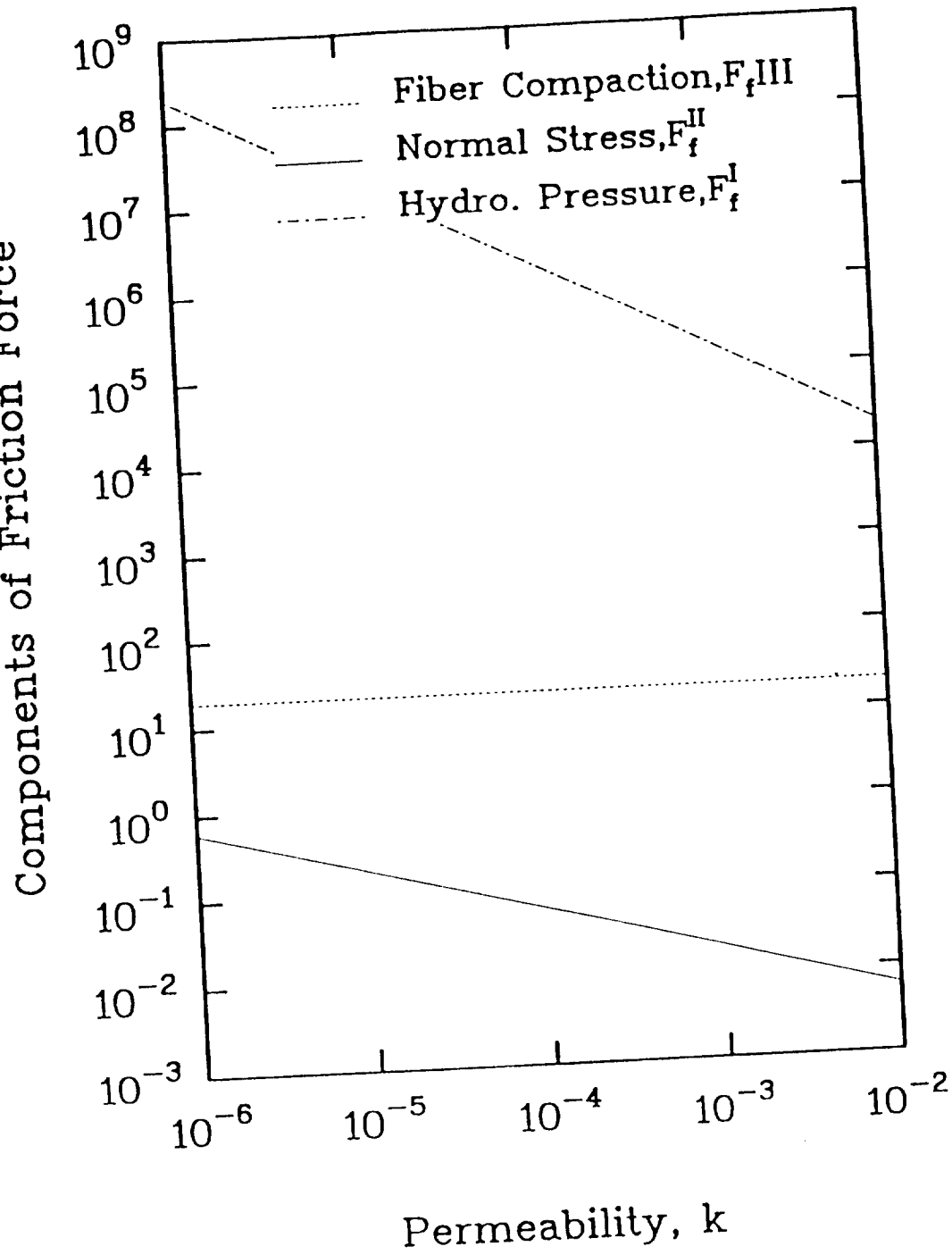

Fig. 3.5 Comparison among Sources of Contribution for Frictional Force; μ_f=0.8, λ=0.98, $kP_{en}(0)$=1.5, R=6.35×10^{-3}m and L=0.3048m.

3.1.3 Collimation Force Contribution, F_c

Collimation forces are related to the geometry of the tapered die section near entrance. There are three different sources of contribution: (i) the bulk compaction force, (ii) resin backflow, and (iii) thermal expansion. They are discussed as follows.

3.1.3.1 Back Compaction Force, F_c^c As discussed before, the laminate pultruded through the die experiences continuous contraction in the lateral r-direction due to the tapered geometry near the die entrance ($-\alpha L \le z \le 0$). Elastic force of the fiber bundles increases fiber volume fraction. This elastic force acts perpendicularly to the surfaces of the tapered die wall. We have for the bulk compaction force F_c^c:

$$F_c^c = (F_c^c)_T = 2\pi \int_{-\alpha L}^{0} P_{fe}(z)\, h(z) \sin\phi dz \quad \text{(dimensional)} \tag{3.25}$$

The dimensionless form of Eq. (3.25) is

$$F_c^c = 2\pi\left(-\frac{\alpha}{\epsilon - 1}\right) \int_{\epsilon}^{1} P_{fe}(h) h \sin\phi dh \tag{3.26}$$

with $\phi = \tan^{-1}[(\epsilon - 1)/\alpha]$ and

$$P_{fe}(h) = \{\frac{\epsilon - h}{\left[1 - \left(\frac{\epsilon - h}{\epsilon - h(\infty)}\right)\right]^n}\} \tag{3.27}$$

where $h(z) = 1 - z\left(\frac{\epsilon - 1}{\alpha}\right)$, $-\alpha \le z \le 0$.

In order to compare magnitudes of various force contributions, an additional dimensionless force term $\tilde{F}_c^c$ is used. Then, with the underscore bar neglected, a dimensionless form of Eq. (3.26) becomes:

$$\tilde{F}_c^c = 2\pi\left(-\frac{\alpha}{\epsilon - 1}\right) \int_{\epsilon}^{1} \tilde{P}_{fe}(h) h \sin\phi \, dh \tag{3.28}$$

or

$$\tilde{F}_c^c = 2\pi \tilde{K}_{FENEC}\left(-\frac{\alpha}{\epsilon-1}\right)\int_{\epsilon}^{1}\left\{\frac{\epsilon-h}{\left[1-\frac{\epsilon-h}{\epsilon-h(\infty)}\right]^n}\right\} h \sin\phi \, dh \tag{3.29}$$

where values of n, α, ϵ and $h(\infty)$ are given in Table 2.2.

3.1.3.2 Backflow Force Contribution, F_c^b The dimensionless pressure profile $P_b(z)$ in the tapered section of the die generated by the resin backflow is given by Eq. (2.8). Thus, we have

$$F_c^b = \left(F_c^b\right)_T = 2\pi \int_{-\alpha L}^{0} P_b(z)\, h(z) \sin\phi \, dz \quad \text{(dimensional)} \tag{3.30}$$

Using the relations for $\underline{F}_c^b$ and $\underline{P}_c$ as given before, the dimensionless form of Eq. (3.30) without the underscore bar is expressed as

$$F_c^b = 2\pi \int_{-\alpha}^{0} \left(\frac{L}{R}\right) P_b(z)\left[1-\left(\frac{\epsilon-1}{\alpha}\right)z\right] \sin\phi \, dz \tag{3.31}$$

where $\phi = \tan^{-1}[(\epsilon-1)/\alpha]$.

3.1.3.3 Thermal Expansion Force Contribution, F_c^k The relation for F_c^k is given by

$$F_c^k = \left(F_c^k\right)_T + \left(F_c^k\right)_M$$

$$= 2\pi \int_{-\alpha L}^{0} P_T(z)\, h(z) \sin\phi \, dz + 2\pi\mu_f \int_{0}^{L} P_T(z) h(z) \cos\phi dz \quad \text{(dimensional)} \tag{3.32}$$

The dimensionless form of Eq. (3.32) is

$$F_c^k = 2\pi\left(\frac{L}{R}\right)\int_{-\alpha}^{0} P'_T(z) h(z) \sin\phi dz + 2\pi\left(\frac{L}{R}\right)\mu_f \int_{0}^{1} P'_T(z) h(z) \cos\phi dz$$

$$= 2\pi\left(\frac{L}{R}\right)\int_{-\alpha}^{0} P_T'(z)\left[1-\left(\frac{\epsilon-1}{\alpha}\right)z\right]\sin\phi dz$$

$$+2\pi\left(\frac{L}{R}\right)\mu_f\int_{0}^{1} P_T'(z)[1-(1-\lambda)z]\cos\phi dz \qquad (3.33)$$

where ϕ is as defined in Eq. (3.31). The dimensionless form of $P_T'(z)$ is given by

$$P_T'(z) = \frac{\alpha_v}{k_c}\frac{R^2}{\mu L v_f}(T_{pul}-T_{amb})\left(1+\frac{z}{\alpha}\right)\ (-\alpha \le z \le 0) \qquad (3.34)$$

Substitute Eq. (3.34) into Eq. (3.33), an analytical solution in the closed form is obtained as

$$F_c^k = 2\pi\left(\frac{\alpha_v}{k_c}\right)\left(\frac{R}{\mu v_f}\right)(T_{pul}-T_{amb})$$
$$\left\{\left[\frac{\alpha}{2}+\frac{\alpha(\epsilon-1)}{6}\right]\left[\sin\phi+\mu_f\cos\phi\right]+\frac{1}{2}\mu_f(1+\lambda)\right\} \qquad (3.35)$$

The thermal force contribution F_c^k can be estimated by the values of pultrusion parameters given in Table 2.2. The comparison among the collimation forces is shown in Fig. 3.6.

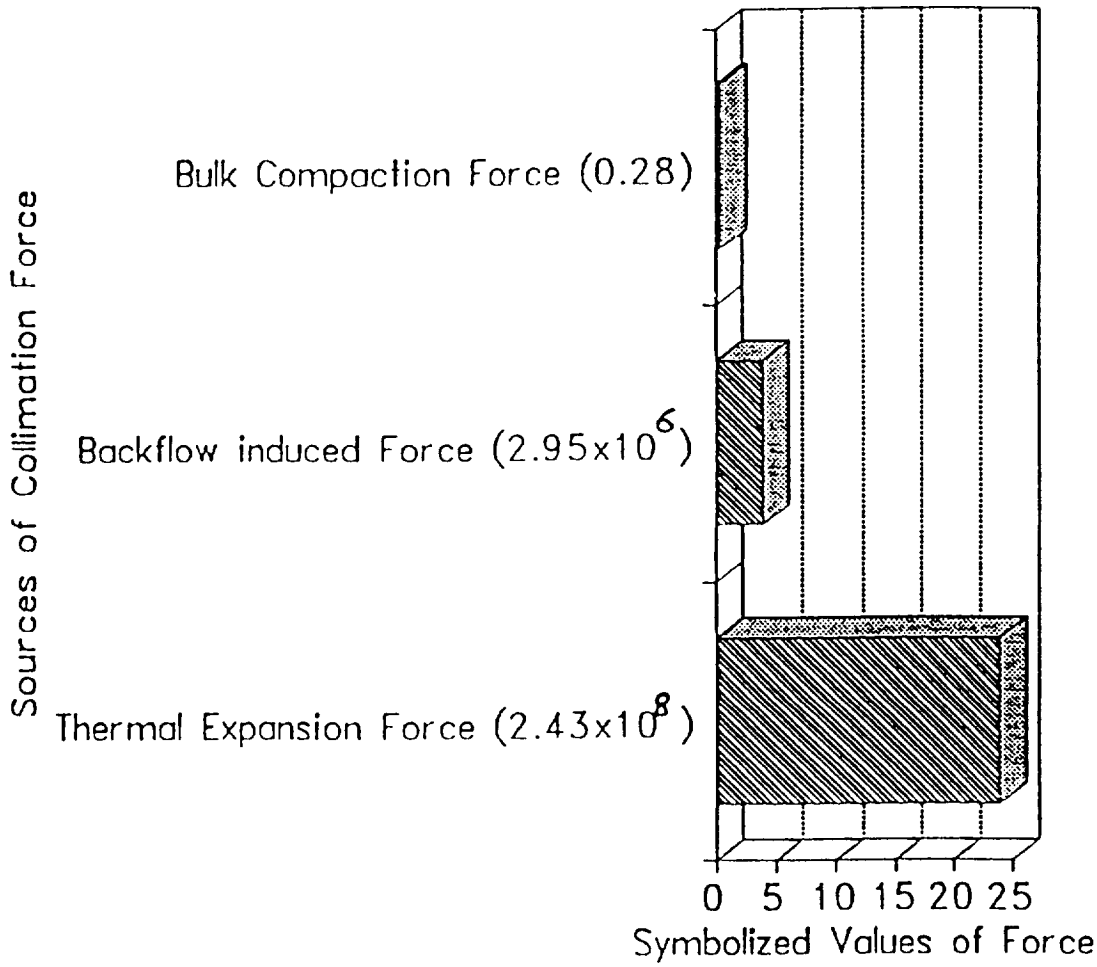

Fig. 3.6 Comparison among the Collimation Forces; α=0.1, ϵ=1.5, V_o=0.25, ΔT=200°C, D_f=0.002, S_z=1, $\alpha_v=5\times10^{-5}$ °C^{-1}, $\kappa_c=5\times10^{-10}$m^{2}N^{-1}, $\mu=0.14P_aS_{ec}$, R=9.525×10^{-3}m, L=0.203m, $v_f=6.35\times10^{-3}$m/sec, k=9.19×10^{-6}, $P_{en}(0)=1.798\times10^5$, μ_f=0.8, $K_{FENEC}=2.72\times10^7$, n=1.5, h(∞)=0.87 and $V_f(\infty)$=0.74.

3.2 Discussion

Total pulling force for the pultrusion process is the sum of contributions from viscous drag, F_v, frictions F_f, and the collimation force F_c. Thus, F_{total} is given by

$$\begin{aligned} F_{total} &= F_v + F_f + F_c \\ &= F_v + F_f^I + F_f^{II} + \left(F_f^{III}\right)_T + \left(F_f^{III}\right)_M \\ &\quad + F_c^c + F_c^b + \left(F_c^k\right)_T + \left(F_c^k\right)_M \end{aligned} \tag{3.36}$$

It is noted that different sources of contribution to the total dimensionless pulling force are functions of various combinations of dimensionless processing, geometry and material parameters. Sets of geometric parameters which affect various force contribution sources are all different. For a given die geometry and prepreg system [17], $F_v, F_f^I, F_f^{II}, and\ F_c^b$ are dependent on the permeability, k, while $\tilde{F}_f^{III}, \tilde{F}_c^c\ and\ F_c^k$ are functions of the pulling speed, v_f. The terms F_f^{III} and F_c^c are written without tilde in Table 3.2. The comparison among the different sources of pultrusion process force is shown in Fig. 3.7.

Table 3.2 Forces with Explicit Pultrusion Process Parameters

Forces	Processing	Geometry	Material
F_v	$kP_{en}(0)$	λ	k
F_f^I	$kP_{en}(0)$	λ, L/R	k, μ_f
F_f^{II}	$kP_{en}(0)$	λ, L/R, ϵ, α	k, μ_f
F_f^{III}	v_f	λ, ϵ, α, R	μ, n, h(∞), μ_f, K_{FENEC}
F_c^c	v_f	ϵ, α, R	μ, n, h(∞), K_{FENEC}
F_c^b		ϵ, α, L/R	k, V_o, D_f, S_z
F_c^k	$(T_{pul}-T_{amb})$, v_f	ϵ, α, L/R	μ, α_v, κ_c

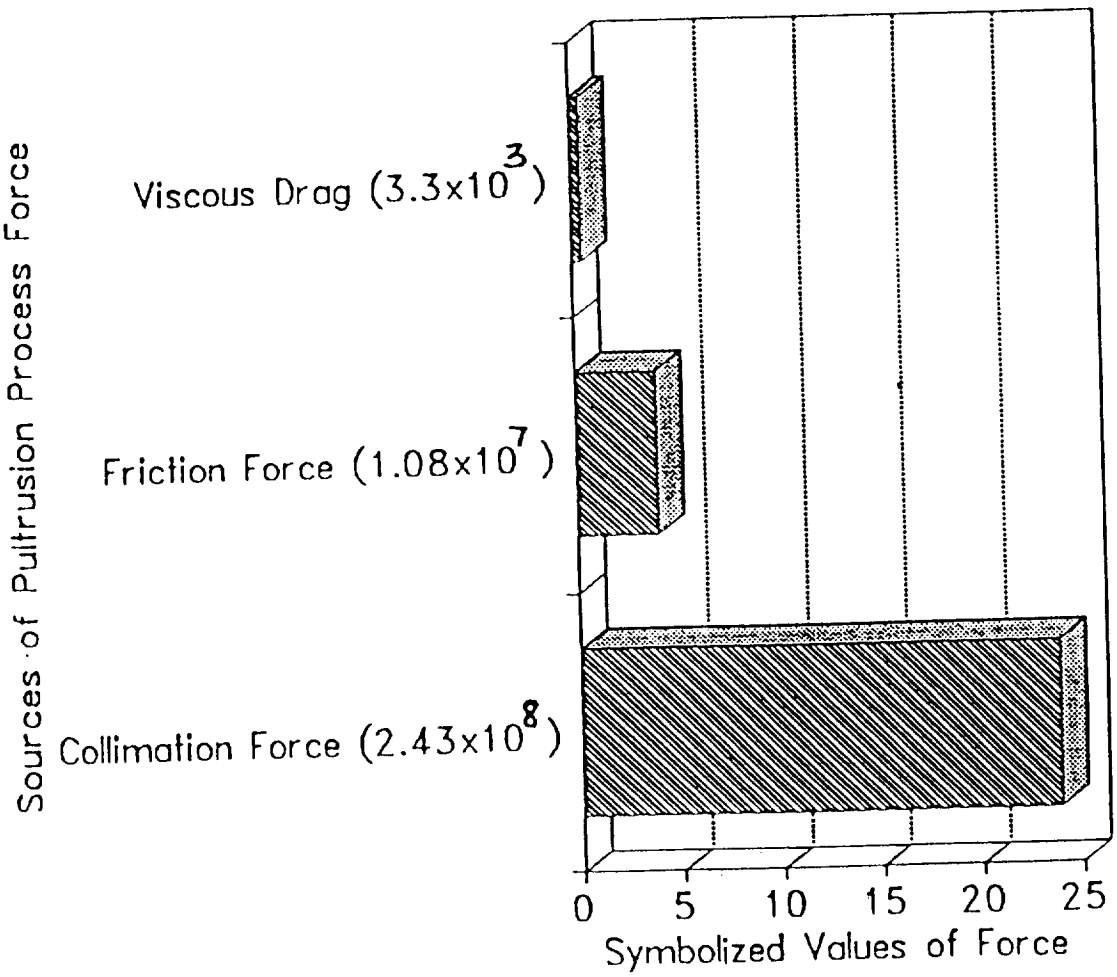

Fig. 3.7 Comparison among the Main Pultrusion Process Forces; α=0.1, ϵ=1.5, V_o=0.25, ΔT=200°C, D_f=0.002, S_z=1, $\alpha_v=5\times10^{-5}$ °C^{-1}, $\kappa_c=5\times10^{-10}$m^{2}N^{-1}, $\mu=0.14P_aS_{ec}$, R=9.525×10^{-3}m, L=0.203m, $v_f=6.35\times10^{-3}$m/sec, k=9.19×10^{-6}, $P_{en}(0)=1.798\times10^{5}$, μ_f=0.8, $K_{FENEC}=2.72\times10^{7}$, n=1.5, h($\infty$)=0.87 and $V_f(\infty)$=0.74.

Chapter 4

VISCOUS HEATING

The generation of heat due to the action of viscous dissipation can lead to significant temperature variations across the shear fields in any of viscometer configurations. For Newtonion fluid with temperature independent properties, with an isothermal wall, the temperature profile will be shown in the next chapter. This case is thought of as a simplest case for the study of the effect of viscous heating with constant viscosity.

4.1 Calculation of Viscous Heating

The viscous heating is used in high viscous flows. It is predicted by an empirical equation, which is a simplified form of the conservation equation of energy. For nondimensionalizing the energy equation, additional dimensionless terms are introduced as follows:

$\underline{T}_o = T/T_o$, B_r(Brinkman number)$=\mu_f{}^2/(K_c T_o)$, R_e(Reynolds number)$=\rho v_f R/\mu$,

Pr(Prandtl number)$=\mu C_p/K_c$.

4.1.1 Governing Equation

The energy equation in terms of T_o and C_p is given as

$$\rho c_p \frac{DT}{Dt} = -(\nabla \cdot q) - (\tau \cdot \nabla v) \qquad \text{(dimensional)} \tag{4.1}$$

For constant ρ, K_c, and C_p, Eq. (4.1) is expressed as

$$\rho c_p \frac{DT}{Dt} = K_c \nabla^2 T + \frac{1}{2}\mu(\dot{\gamma} \cdot \dot{\gamma}) \tag{4.2}$$

where K_c is the heat conductivity defined as heat flow across a unit area when temperature gradient is unity (Btu/(tLT)). The symbol C_p is the heat capacity at constant pressure per unit mass (Btu/(MT)), and $\dot{\gamma} = \left[\nabla\vec{v} + (\nabla\vec{v})^T\right]$.

By noting that $v_r=v_r(r)$ and $T=T(z,r)$. Eq. (4.2) is expressed in a dimensionless form as

$$R_eP_r\{v_r\frac{\partial T}{\partial r} + \left(\frac{R}{L}\right)v_z\frac{\partial T}{\partial z}\} = \frac{\partial^2 T}{\partial r^2} + \frac{1}{r}\frac{\partial T}{\partial r} + \left(\frac{R}{L}\right)^2\frac{\partial^2 T}{\partial z^2} + B_r\left(\frac{dv_z}{dr}\right)^2 + 2B_r\{\left(\frac{\partial v_r}{\partial r}\right)^2 + \left(\frac{v_r}{r}\right)^2 + \left(\frac{R}{L}\right)^2\left(\frac{\partial v_z}{\partial z}\right)^2\} \quad (4.3)$$

Further, it is assumed that heat conduction in the longitudinal (fiber) direction is negligible, the velocity gradient ($\alpha v_r/\alpha r$)>>dv_z/dz), and the secondary flow, $v_r(r)$, inside the die is negligibly small. Thus, Eq. (4.3) reduces to

$$\frac{\partial^2 T}{\partial r^2} + \frac{1}{r}\frac{\partial T}{\partial r} - R_eP_r\left(\frac{R}{L}\right)v_z\frac{\partial T}{\partial z} + B_r\left(\frac{dv_z}{dr}\right)^2 = 0 \quad (4.4)$$

Equation (4.4) is solved for (dimensionless) temperature decrease due to viscous heating .

4.1.2 Boundary Conditions

For steady state flow condition (assumption) and T=T(r,z), the following boundary conditions are specified:

At $r = 0$, $\partial T/\partial r = 0$ (dimensional)

At $r = h$, $T = T_0$ (dimensional)

The dimensionless form of the boundary conditions are given as

At $r = 0$, $\partial T/\partial r = 0$

At $r = h$, $T = 1$

4.2 Discussion

This problem is solved by the finite element method. The procedures and results are presented in Chap. 5.

Chapter 5

FINITE-ELEMENT METHOD THERMAL ANALYSIS FOR THE PULTRUSION PROCESSING

The finite element method is selected as a numerical approach to carry out the solution of the physical problem. In this method, mathematical formulations are displayed explicitly in a sequence of representations of the integral equations with continuous boundary conditions. These are different from the finite difference method which is applied in solving the problems where mathematical formulations are given by differential equations. In the thermal analysis for the pultrusion processing, the finite difference method (which is suited to solve fluid dynamics problems in rectangular boxes) is not applicable in general. In this study, the two-dimensional heat transfer equation with cylindrical coordinates is solved by a finite element method [18].

5.1 Introduction

The analysis of thermoplastic pultrusion includes the derivation of equation for the velocity distribution, resin pressure, pulling force and heat transfer in the processing. It now remains investigation of the temperature profile in the system. The temperature profile can be obtained by conducting experiments. It can also be obtained by solving the energy equation using the Galerkin Finite Element Method. The assumption made in isothermal heating condition for the process leads to the boundary conditions that are easier to define. Also, the symmetric die design shape provides convenience for the temperature evaluation by the Finite Element Method. For simplicity, the assumptions of low viscous heating and a Newtonian fluid is made for the following analyses. The detailed formulations and numerical examples for the problem is given next in order to

demonstrate the applicability of the finite element methods for heat transfer analysis of the pultrusion processing.

5.2 Governing Differential Equation

The governing differential equations for thermal energy transfer analysis associated with the pultrusion processing are summarized as follows:

$$\left(\frac{R}{L}\right)^2\frac{\partial^2 T}{\partial z^2}+\frac{\partial^2 T}{\partial r^2}+\frac{1}{r}\frac{\partial T}{\partial r}-R_e P_r\left(\frac{R}{L}\right)v_z\frac{\partial T}{\partial z}+B_r\left(\frac{\partial v_z}{\partial r}\right)^2=0 \qquad (5.1)$$

where $h = 1 - z(1 - \lambda)$. The velocity profile v_z(z,r) is defined along the flow direction, the z-direction, as

$$v_z(z,r)=\{1-2[1-kP_{en}(0)]z\}\left[1-\frac{I_o\left(\frac{r}{\sqrt{k}}\right)}{I_o\left(\frac{h}{\sqrt{k}}\right)}\right] \qquad (5.2)$$

where I_o is the modified Bessel function of zero order of the first kind. Velocity gradient along r-direction is given as

$$\frac{\partial v_z(z,r)}{\partial r}=-\frac{1}{\sqrt{k}}\{1-2[1-kP_{en}(0)]z\}\left[\frac{I_1\left(\frac{r}{\sqrt{k}}\right)}{I_o\left(\frac{h}{\sqrt{k}}\right)}\right] \qquad (5.3)$$

where I_1 is the modified Bessel function of order one of the first kind.

The boundary conditions for the low viscous heating of Newtonian fluids pultrusion are given as

$$T(0,r) = 1, \text{ at z=0}$$

$$T(1,r) = 1, \text{ at z=1}$$

$$T(z,h) = 1, \text{ at r=h}$$

$$\frac{\partial T}{\partial r}(z,0) = 0, \text{ at r=0}$$

where z=0 and z=1 represent the locations at the inlet and the outlet of the flow processing, respectively; and r=0 and r=h represent the locations at the center line and the surface of the flow domain, respectively.

5.3 Finite Element Modeling

The following discussion focuses on formulating the finite element modeling. The fluid domain is first divided into eight-nodes quadrilateral elements. In the finite element method, the field variable which is temperature in this case , is interpolated as the product of shape functions N_i and nodal degrees of freedom, T_i, as

$$T^{(e)} = \sum_{i=1}^{8} N_i T_i^{(e)} = \mathbf{N}^{\mathrm{T}}\mathbf{T} \tag{5.4}$$

where N_i, T_i are functions of r and z.

The Galerkin Finite Element method invokes the condition that the weighted residuals of the governing differential equations are zero, i.e.,

$$\int_{\Omega^e} N_i \cdot \left(\left(\frac{R}{L}\right)^2 \frac{\partial^2 T}{\partial z^2} + \frac{\partial^2 T}{\partial r^2} + \frac{1}{r}\frac{\partial T}{\partial r} - R_e P_r \left(\frac{R}{L}\right) v_z \frac{\partial T}{\partial z} + B_r \left(\frac{\partial v_z}{\partial r}\right)^2\right) d\Omega = 0,$$
$$i = 1, 2, \cdots 8 \tag{5.5}$$

This leads to a matrix equation in terms of nodal temperature, T_i. Upon substituting Eq. (5.4) into Eq. (5.5) and integrating the resultant equation by parts, the final equation is obtained as

$$\sum_{j=1}^{8} \int_{\Omega^e} \left\{ \frac{\partial N_i}{\partial r}(r)\frac{\partial N_j}{\partial r} + \frac{\partial N_i}{\partial z}\left[\left(\frac{R}{L}\right)^2 (r)\right]\frac{\partial N_j}{\partial z} + R_e P_r \left(\frac{R}{L}\right) r N_i v_z \frac{\partial N_j}{\partial z} \right\} d\Omega(T_j)$$
$$= \int_{\Omega^e} N_i(r) B_r \left(\frac{\partial v_z}{\partial r}\right)^2 d\Omega,$$
$$i = 1, 2, \cdots 8 \tag{5.6}$$

The area integals defined in Eq. (5.6) can be numerically evaluated by using the technique of 3x3 Gaussian quadrature. Specifically, one can define the components of the local stiffness matrices and the force vector as

$$K_{ij}^{a} = \int_{\Omega} \left\{ \frac{\partial N_i}{\partial r}(r)\frac{\partial N_j}{\partial r} + \frac{\partial N_i}{\partial z}\left[\left(\frac{R}{L}\right)^2 \cdot (r)\right]\frac{\partial N_j}{\partial z} \right\} d\Omega \tag{5.7}$$

$$K_{ij}^{b} = \int_{\Omega^e} \left\{ R_e \cdot P_r \cdot \left(\frac{R}{L}\right) \cdot r \cdot N_i \cdot v_z \frac{\partial N_j}{\partial z} \right\} d\Omega \tag{5.8}$$

$$F_i = \int_{\Omega^e} N_i \cdot r \cdot B_r \cdot \left(\frac{\partial v_z}{\partial r}\right)^2 d\Omega \tag{5.9}$$

where i=1.....8, j=1.....8.

The technique of 3x3 Gaussian quadratures maps physical domain Ω^e of Fig. 5.1 to a square bounded by $-1 \le s \le 1$ and $-1 \le t \le 1$. In this case, the shape functions are mapped to:

$$N_1(s,t) = .25(1-s)(1-t)(-1-s-t)$$

$$N_2(s,t) = .25(1+s)(1-t)(-1+s-t)$$

$$N_3(s,t) = .25(1+s)(1+t)(-1+s+t)$$

$$N_4(s,t) = .25(1-s)(1+t)(-1-s+t)$$

$$N_5(s,t) = .25(1-s\times s)(1-t)$$

$$N_6(s,t) = .25(1+s)(1-t\times t)$$

$$N_7(s,t) = .25(1-s\times s)(1+t)$$

$$N_8(s,t) = .25(1-s)(1-t\times t)$$

where s, t are dimensionless coordinates after mapping transformation from r, z. Next, the integration of equations Eqs. (5.7–5.9) is performed to obtain the local stiffness matrices as

$$\mathbf{K_a} = \int_{-1}^{1}\int_{-1}^{1} \mathbf{D}(s,t)\Theta(s,t)\mathbf{D}^{\mathrm{T}}(s,t)dsdt$$

$$\mathbf{K_b} = \int_{-1}^{1}\int_{-1}^{1} \mathbf{N}(s,t)\mathbf{V}^{\mathrm{T}}\mathbf{N}(s,t)\mathbf{L}(s,t)\mathbf{D}^{\mathrm{T}}(s,t)dsdt$$

and for the force vector as

$$\mathbf{F} = \left[\int_{-1}^{1}\int_{-1}^{1} \mathbf{N}(s,t)\mathbf{N}^{\mathrm{T}}(s,t)|\mathbf{J}|\, dsdt\right] \mathbf{H}$$

The D matrix appearing in K_a and K_b is given as

$$\mathbf{D} = \begin{bmatrix} \frac{\partial \mathbf{N}}{\partial s} & \frac{\partial \mathbf{N}}{\partial t} \end{bmatrix} = \begin{bmatrix} \frac{(1-t)(2s+t)}{4} & \frac{(1-s)(s+2t)}{4} \\ \frac{(1-t)(2s-t)}{4} & \frac{(1+s)(-s+2t)}{4} \\ \frac{(1+t)(2s+t)}{4} & \frac{(1+s)(s+2t)}{4} \\ \frac{(1+t)(2s-t)}{4} & \frac{(1-s)(-s+2t)}{4} \\ -s(1-t) & \frac{-(1-s^2)}{2} \\ \frac{(1-t^2)}{2} & -t(1+s) \\ -s(1+t) & \frac{(1-s^2)}{2} \\ \frac{-(1-t^2)}{2} & -t(1-s) \end{bmatrix} \tag{5.10}$$

The matrix given by Eq. (5.10) represents the gradients of shape functions. The Jacobian matrix **J** is defined as

$$\mathbf{J} = \begin{bmatrix} z_e^T \frac{\partial \mathbf{N}}{\partial s} & r_e^T \frac{\partial \mathbf{N}}{\partial s} \\ z_e^T \frac{\partial \mathbf{N}}{\partial t} & r_e^T \frac{\partial \mathbf{N}}{\partial t} \end{bmatrix} \tag{5.11}$$

where the partial derivatives of the shape functions have been selected in terms of s, t coordinates as

$$\frac{\partial \mathbf{N}^\mathbf{T}}{\partial z} = \mathbf{J_1} \frac{\partial \mathbf{N}^\mathbf{T}}{\partial s} = \mathbf{J_1 D}^\mathbf{T} \tag{5.12}$$

and

$$\frac{\partial \mathbf{N}^\mathbf{T}}{\partial r} = \mathbf{J_2} \frac{\partial \mathbf{N}^\mathbf{T}}{\partial s} = \mathbf{J_2 D}^\mathbf{T} \tag{5.13}$$

where $\mathbf{J_1}$ and $\mathbf{J_2}$ are, respectively, the first and second rows of inverse of the Jacobian matrix **J**. The velocity vector **V** is a function of constant v_z which can be written approximately as

$$v_z \approx \mathbf{N}^\mathbf{T} \mathbf{v_z}$$

The velocity vector **V** is then defined as

$$\mathbf{V} = R_e \cdot P_r \cdot \mathbf{v_z} \cdot r \cdot R/L$$

The same relation can be applied to represent $\partial v_z / \partial r$. As a result, one can define matrix H appearing in F as

$$\mathbf{H} = (r \cdot B_r(\partial v_z/\partial r)^2)$$

The matrix $\mathbf{L}$ is defined as $\mathbf{L} = \mathbf{J_1}|\mathbf{J}|$, where $|\mathbf{J}|$ is determinant of the Jacobian matrix. Moreover, the Θ matrix appearing in K_a is given as

$$\Theta = \mathbf{J}|\mathbf{J}| = [\mathbf{J}_1^T\mathbf{J}_1\left(\frac{R}{L}\right)^2 \cdot r + \mathbf{J}_2^T\mathbf{J}_2 \cdot r]|\mathbf{J}| \tag{5.14}$$

Finally, using 3×3 Gaussian points, the integrals for K_a, K_b and F can be simplified as

$$\mathbf{K}_a \approx \left[\sum_{i=1}^{3}\sum_{j=1}^{3} W_i W_j \mathbf{D}_{ij}(\Theta)_{ij}\mathbf{D}_{ij}^T\right] \tag{5.15}$$

$$\mathbf{K}_b \approx \left[\sum_{i=1}^{3}\sum_{j=1}^{3} W_i W_j \mathbf{N}_{ij}\mathbf{V}^T\mathbf{N}_{ij}\mathbf{L}_{ij}\mathbf{D}_{ij}^T\right] \tag{5.16}$$

and

$$\mathbf{F} \approx \left[\sum_{i=1}^{3}\sum_{j=1}^{3} W_i W_j \mathbf{N}_{ij}\mathbf{N}_{ij}^T|J|_{ij}\right]\mathbf{H} \tag{5.17}$$

where subscripts i and j refer to the Gaussian points in the three-point Gaussian quadratures along s axis and t axis. The weighing coefficients W_1= W_2= W_3= 5/9 and s_i=-.774597, 0, .774597 for i=1 to 3, and t_j=-.774597, 0, .774597 for j=1 to 3.

After assembling the above local matrices, one obtains a global matrix equation:

$$(\mathbf{K}_a + \mathbf{K}_b)\mathbf{T} = \mathbf{F} \tag{5.18}$$

where $\mathbf{K}_a$ and $\mathbf{K}_b$ are associated with heat conduction and heat convection , respectively. Standard process such as LU factorization can be used to solve the above equations for nodal values of temperature.

5.4 Numerical Example

To verify the finite element procedure proposed in the last section, a simple heat transfer problem is presented here. The domain of the problem is a rectangular configuration shown in Fig. 5.1, which is discretized into 12 elements and 51 nodes with specified boundary conditions.

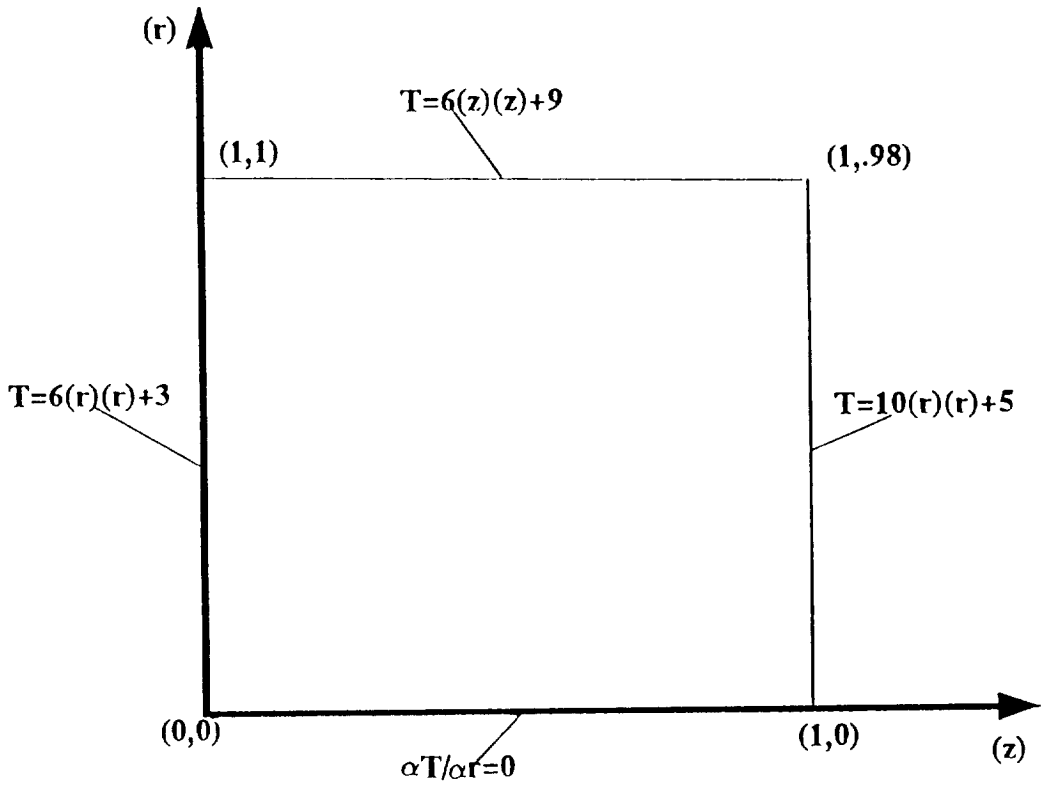

Fig. 5.1 Boundary Conditions for Numerical Example.

The heat transfer problem is governed by the following differential equation:

$$\left(\frac{R}{L}\right)^2 \frac{\partial^2 T}{\partial z^2} + \frac{\partial^2 T}{\partial r^2} + \frac{1}{r}\frac{\partial T}{\partial r} - a(r,z)\frac{\partial T}{\partial z} + f(r,z) = 0 \quad (dimensionless) \tag{5.19}$$

where a(r, z) and f(r, z) are given by

$$a(r,z) = R_e P_r \left(\frac{R}{L}\right)\{1 - 2[1 - kp_{en}(0)]z\}[1 - \frac{I_0\left(\frac{r}{\sqrt{k}}\right)}{I_0\left(\frac{h}{\sqrt{k}}\right)}] \tag{5.20}$$

and

$$\mathrm{f(r,z)} = -\left(\frac{\mathrm{R}}{\mathrm{L}}\right)^2 4\left(2\mathrm{r}^2 + 1\right) - 8\left(2\mathrm{z}^2 + 3\right) + \mathrm{a(r,z)}4\mathrm{z}\left(2\mathrm{r}^2 + 1\right) \tag{5.21}$$

Equation (5.19) is very similar to Eq. (5.1) with a(r, z) and f(r, z) related to v_z and $\partial v_z/\partial r$, respectively. The exact solution of Eqs. (5.19–5.21) is

$$\mathrm{T(r,z)} = \left(2\mathrm{z}^2 + 3\right)\left(2\mathrm{r}^2 + 1\right) \tag{5.22}$$

if the boundary conditions of the problem are specified as:

$$\mathrm{z} = 0,\ \mathrm{T(r)} = 3\left(2\mathrm{r}^2 + 1\right)$$

$$\mathrm{z} = 1,\ \mathrm{T(r)} = 5\left(2\mathrm{r}^2 + 1\right)$$

$$\mathrm{r} = 1,\ \mathrm{T(z)} = 3\left(2\mathrm{z}^2 + 3\right)$$

$$r = 0,\ \partial T/\partial r = 0$$

Based upon the finite element formulation in Sec. 5.3, the resultant numerical temperature distribution is listed in Table 5.1.

Table 5.1 Comparison between Numerical and Actual Values

Element Number	Exact Temperture	Numerical Temperture	Element Number	Exact Temperture	Numerical Temperture
1	3.000	3.000	27	10.226	10.208
2	3.369	3.369	28	10.292	10.278
3	4.470	4.470	29	10.361	10.360
4	6.308	6.300	30	11.336	11.340
5	8.880	8.880	31	11.185	11.164
6	8.940	8.940	32	5.680	5.694
7	9.000	9.000	33	3.845	4.259
8	9.036	9.036	34	4.280	4.631
9	8.916	8.895	35	4.788	4.763
10	4.494	4.519	36	6.310	6.307
11	3.020	3.586	37	8.854	8.872
12	3.080	3.584	38	12.406	12.364
13	3.454	3.422	39	12.484	12.383
14	4.577	4.588	40	12.568	12.570
15	6.449	6.499	41	13.530	13.530
16	9.069	8.995	42	13.340	13.332
17	9.130	8.846	43	6.802	6.810
18	9.191	9.191	44	4.620	4.853
19	9.644	9.644	45	5.000	5.000
20	9.548	9.507	46	5.590	5.590
21	4.813	4.833	47	7.350	7.350
22	3.245	3.891	48	10.293	10.290
23	3.500	3.835	49	14.417	14.410
24	3.920	3.924	50	14.506	14.510
25	5.182	5.188	51	14.604	14.604
26	7.282	7.282			

The column of the exact temperature consists of data obtained from Eq. (5.22). In the table, it is observed that the maximum difference between the exact value and the finite element solution is about 20% appearing at the fourth boundary. The temperatures obtained by the finite element method in other areas are very close to the exact solution.

5.5 Numerical Results for Pultrusion Processing

The finite element method developed above is applied for thermal analysis of a pultrusion process problem. Due to the symmetry of the problem geometry, only the upper half plane of the flow field is considered for finite element analysis. The finite element mesh is shown in Fig. 5.2, which consists of 12 elements and 51 nodes.

Heat transfer analysis of this pultrusion process is performed and the results are reported in this section. Table 5.2 documents the numerical results obtained by the finite element method given in Sec. 5.3.

In order to evaluate the effect of viscosity in temperature distribution, heat transfer analyses are performed for different $\hat{P}_T(z)$ and B_r which are the processing parameters related to the viscosity. These parameters are expressed as

$$\hat{P}_T(z) = (\alpha_v R^2/\kappa_c \mu L v_f)(T_{pul} - T_{amb})(1 + z/\alpha)$$

and

$$B_r = \mu/(\kappa_c T_o)$$

The numerical study shows that the final temperature distribution is uniform everywhere for the parameters values described in Table 5.2 in which B_r varied from 10^{-4} to 10^4. The factors that affect the temperature distribution in the process include higher curing point and superior toughness. However, these factors were not considered in the present case. As a result, the temperature is uniformly distributed across the die section. In their experimental study, Larock and Hahn [3] also observed the similar phenomenon.

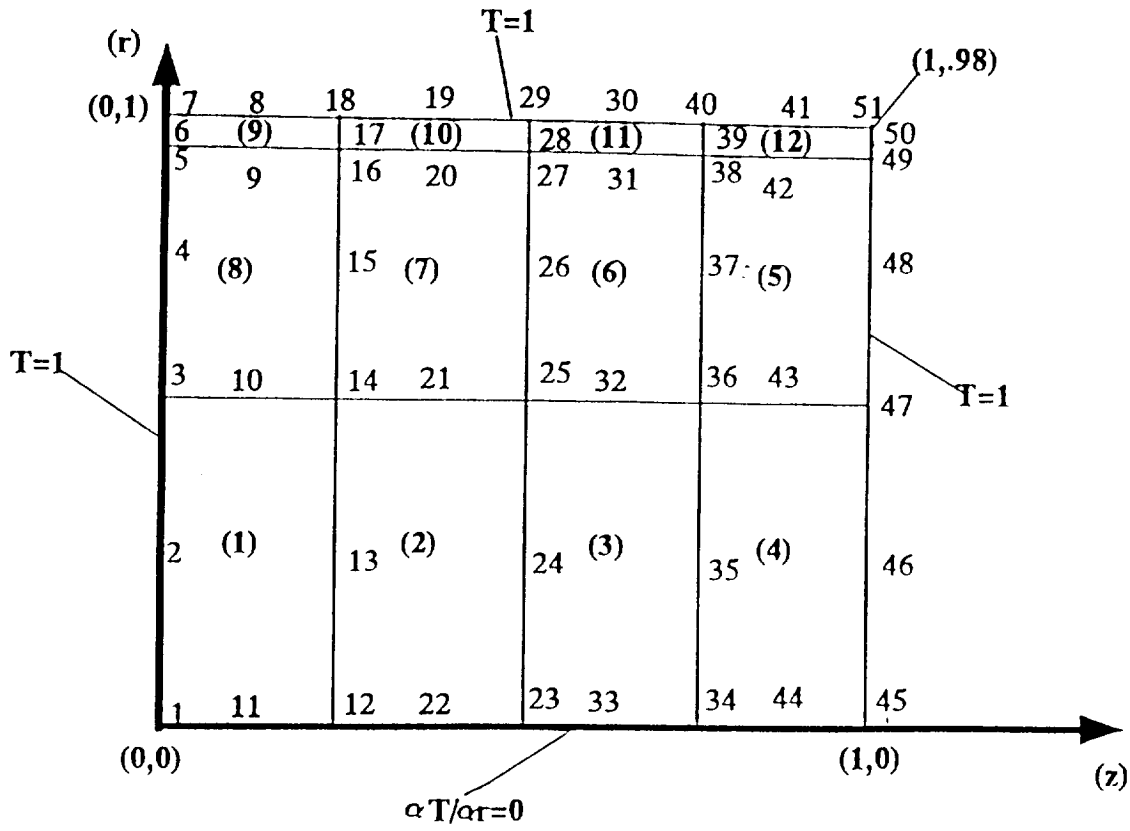

Fig. 5.2 Finite Element Mesh and the Boundary Conditions.

Table 5.2 Key Processing Parameters and Calculation of Temperature Values

viscousity (μ)	Brinkman No. (Br)	KPen(0)	Pen(0)	Permeability (K)	Temp. (T)
0.14	3	1.5	1.5×10^{6}	10^{-6}	1.
14	300	1.5	1.5×10^{4}	10^{-4}	1.
1400	30000	1.5	1.5×10^{2}	10^{-2}	1.

Chapter 6

CONCLUSIONS

Pultrusion processing for long fiber reinforced thermoplastic composite is analyzed theoretically. The pultrusion die consists of two sections: short tapered section near the entrance followed by a main pultrusion die with near constant diameter. The pressure distribution in the entrance section is analyzed, which takes into account the contribution from back flow and thermally induced pressurization effects. It is found that the latter exhibits predominant effect on the pressure built up in the entrance die section.

Flow analysis in the main pultrusion die section is accomplished by using a modified Darcy's law for flow through a porous media. The modified form incorporates viscous stress term which is used to account for distribution of velocity profile near the die wall. Closed form solutions for the velocity and pressure distribution are obtained for the first time. It is found that velocity profile, $v_z(z, r)$, is a function of $kp_{en}(0)$ where k is the dimensionless permeability and $p_{en}(0)$ is the dimensionless pressure at the end of entrance section of the pultrusion die. It is noted $p_{en}(0) \geq 1/k$ is a necessary condition to obtain pressure and velocity distribution in a pultrusion die with physical significance. In practice, this implies that in order to achieve a laminate flow with the pultrusion die, the pressure built up $p_{en}(0)$ has to be greater than the inverse of permeability, 1/k. The velocity profiles at various die sections, z, are found to remain flat until r/R is greater than 0.98.

Pulling forces encountered in the pultrusion of long fiber reinforced thermoplastic composite are also analyzed. Contributions from various sources, namely frictional, viscous, collimation are considered. It is found that viscous drag contribution to the

pulling forces is negligible, and collimation force contribution dominates the total pulling forces.

For taking account of viscous heating, an additional energy equation is formulated. Numerical analysis using finite element method is conducted to obtain temperature and velocity profiles inside the pultrusion die. Within the range of Brinkman number $10^{-4} \leq B_r \leq 10^4$ investigated, the viscous heating is found to be negligible, resulting in a uniform temperature distribution along the cross section of the pultrusion die.

BIBLIOGRAPHY

1. Price, H. L., "Curing and Flow of Thermosetting Resin for Composite Material Pultrusion," Ph.D. Dissertation, Old Dominion University, Norfolk, Virginia, May 1979, pp. 106–110.

2. Tulig, T. J., "A Heat Transfer and Reaction Model for Pultrusion," Proceedings, American Institute of Chemical Engineering (AICHE), Chicago, Illinois, November 1985.

3. Han, C. D., Lee, D. S., and Chin, H. B., "Development of a Mathematical Model for the Pultrusion Process," Polymer Engineering and Science, Vol. 26, No. 6, March 1986, pp. 393–395.

4. Ma, C. C., "The Correlations of Processing Variables for Optimizing the Pultrusion Process," The Society for the Advancement of Material and Process Engineering Journal, Vol. 22, No. 5, 1986, pp. 42–43.

5. Batch, G. L., and Macosko, C. W., Proceedings, 42nd Annual Conference Reinforced Plastics/Composites Institute, The Society of the Plastics Industry, Vol. B12, 1985.

6. Batch , G. L., "Cross-linking Free Radical Kinetics and the Pultrusion Processing of Composites," Ph.D. Dissertation, University of Minnesota, May 1989, pp. 241–246.

7. Summerak, J. E., "Understanding Pultrusion Process Variables for the First Time," Modern Plastics, March 1985, pp. 58–60.

8. Brinkman, H. C., "A Calculation of the Viscous Force Exerted by a Flowing Fluid on a Dense Swarm of Particles," Applied Science Research, Vol. A1, February 1947, pp. 27–34.

9. Brinkman, H. C., "On the Permeability of Media Consisting of Closely Packed Porous Particles," Applied Science Research, Vol. A1, October 1947, pp. 81–86.

10. Bird, R. B., Stewart, W. E., and Lightfoot, E. N., Transport Phenomena, John Wiley & Sons, Inc., 1960, pp. 152–153.

11. Haberman, R., Elementary Applied Partial Differential Equations, Prentice-Hall, Inc., 1987, pp. 242–244.

12. Carman, P. C., Transaction of the American Institute of Chemical Engineers, Vol. 15, 1937, pp. 150–152.

13. Gutowaski, T. G., Cai, Z., Kingery, J., and Wineman, S. J., "Resin Flow/Fiber Deformation Experiments," The Society for the Advancement of Material and Process Engineering Quarterly, Vol. 17, No. 4, July 1986, pp. 54–58.

14. Lam, R. and Kardos, J. L., Polymeric Materials Science and Engineering, American Chemical Society Fall Meeting, Los Angeles, 1988, pp. 1190–1192.

15. Williams, J. G., Morris, C. E. M., and Ennis, B. C., "Liquid Flow Through Aligned Fiber Beds," Polymer Engineering and Science, Vol. 14, June 1974, p. 413.

16. Bird, R. B., Armstrong, R. C., and Assager, O. H., Dynamics of Polymetric Liquids, John Wiley & Sons, Inc., 1977, pp. 270–273.

17. Wilde, D. J., Globally Optical Design, John Wiley & Sons, Inc., 1978.

18. Cook, R. D., Malkus, D. S., and Plesha, M. E., Concepts and Applications of Finite Element Analysis, John Wiley & Sons, Inc., 1988, pp. 108–115.

APPENDIX

MODIFIED BESSEL EQUATION

A modified Bessel equation is

$$\frac{d^2y}{dx^2} + \frac{1}{x}\frac{dy}{dx} - \left(\alpha^2 + \frac{n^2}{x^2}\right)y = 0$$

A complete solution of this equation is

$$y = c_1 I_n(\alpha x) + c_2 K_n(\alpha x) \text{ for any n.}$$

where $I_0(0) = 1, I_1(0) = 0, K_o(0) = K_1(0) = \infty$. For n=0,1,2.....an integer, we have

$$I_n(x) = I_{-n}(x) = \frac{x^n}{2^n n!}\{1 + \frac{x^2}{2^2 1!(n+1)} + \frac{x^4}{2^4 2!(n+1)(n+2)} + \frac{x^6}{2^6 3!(n+1)(n+2)(n+3)} + ..\} \quad (A.1)$$

Following theorems can be established

$$\frac{d}{dx}[x^n I_n(x)] = x^n I_{n-1}(x), \quad \frac{d}{dx}[x^{-n} I_n(x)] = x^{-n} I_{n+1}(x)$$

$$\frac{d}{dx}[x^n K_n(x)] = -x^n K_{n-1}(x), \quad \frac{d}{dx}[x^{-n} K_n(x)] = -x^{-n} K_{n+1}(x)$$